neous method for detection of protein–DNA binding and screening of drugs targeting DNA-binding proteins.

Materials and Methods

Oligonucleotides. The following probe oligonucleotides were made for NF-κB-DSE-FRET (F, 6FAM; D, DABCYL; lowercase letters, single-stranded tail; underline, NF-κB binding site): 5′-FAG TTG AGG GGA CTT TCC CAG GCG ACT CAC TAT AGG Cgg tgt ctc gct cgc-3′ (NF-01F), 5′-AGT TGA GGG GAC TTT CCC AGG CGA CTC ACT ATA GGc acc aca cca ttc cc-3′ (NF-13), 5′-ggg aat ggt gtg gtG CCT ATA GTG AGT CGC CTG GGA AAG TCC CCT CAA CTD-3′ (NF-14D), 5′-gcg agc gag aca ccG CCT ATA GTG AGT CGC CTG GGA AAG TCC CCT CAA CT-3′ (NF-02). To prepare probes, 0.5 μM of each oligonucleotide was mixed in annealing buffer (10 mM HEPES-NaOH [pH 7.9], 50 mM KCl, 0.1 mM EDTA), denatured for 2 min at 95°C, and then cooled gradually to allow annealing. Duplexes were stored at 4°C and diluted with binding buffer (10 mM HEPES–NaOH [pH 7.9], 50 mM KCl, 0.1 mM EDTA, 2.5 mM DTT, 10% glycerol, 0.05% Nonidet P40) before use. Oligonucleotides were purchased from Japan Bio Services (Saitama, Japan). All other chemicals were reagent grade or better and were obtained from Wako (Tokyo, Japan).

Protein preparation and DNA binding assay. The GST-fusion recombinant human NF-κB proteins (p50, p52) were expressed and purified[13] and glutathione was removed by dialysis. In general, DNA-binding experiments were carried out in the following manner: 5 μL NF-D1 (consisting of NF-01F and NF-14D) and 5 μL protein in binding buffer were incubated in a 96-well (half-area) microplate for 30 min at room temperature. Next, 40 μL NF-D2 (consisting of NF-02 and NF-13) was added and allowed to incubate for another 60 min at room temperature. Fluorescence was measured at 535 nm after excitation at 485 nm using an EnVision microplate reader (Perkin-Elmer, Waltham, MA, USA). In experiments with inhibitor, 0.5 μL inhibitor, 5 μL NF-D1, and 4.5 μL protein in binding buffer were incubated before addition of 40 μL NF-D2.

To obtain an IC_{50}, the following equation was solved using the "solver" add-on in Microsoft Excel:

$$Y = A + \frac{B - A}{1 + \left(\frac{X}{IC_{50}}\right)^{C}} \quad (1)$$

where Y is the observed fluorescence, X is the inhibitor concentration, A is the lowest fluorescence, B is the highest fluorescence, and C gives the largest absolute value of the slope of the curve.

S/B was obtained by the following formula:

$$S/B = \frac{A}{P} \quad (2)$$

where A is the mean fluorescence of four wells in the absence of protein and P is the mean florescence of four wells in the presence of protein.

Z'-factors were obtained as follows:

$$Z'\text{-factor} = 1 - \frac{3 \times SD_A + 3 \times SD_P}{A - P} \quad (3)$$

where A is the mean fluorescence value of four wells without protein, P is the mean florescence of four wells with protein, SD_A is the standard deviation of A, and SD_P is the standard deviation of P.

Results

The principle of DSE-FRET is illustrated in Figure 1. Two partially double-stranded DNA probes, named D1 and D2, are used. Each probe has a double-stranded region containing a protein binding site and two single-stranded tails. One strand of D1 is labeled with a fluorophore at the 5′-end and the other is labeled with a quencher at the 3′-end. The fluorophore and quencher are placed at the same end of the double-stranded region; therefore, the fluorescence of the fluorophore is quenched. The tails of D1 are complementary to those of D2, so that D1 hybridizes with D2 to form a four-way structure. As the double-stranded regions of the two probes have identical sequences, the junction of the structure migrates spontaneously, followed by irreversible dissociation to give two fully double-stranded duplexes. In other words, strand exchange occurs between D1 and D2. As a result, the quencher-labeled strand of D1 is exchanged for its non-labeled counterpart in D2; therefore, fluorescence is restored. DNA-binding proteins bind to the duplex and block strand exchange, thereby suppressing the fluorescence elevation.

To illustrate the method, we attempted to detect the NF-κB (p50) interaction with DNA. Nuclear factor-κB plays a pivotal role in the coordinated transcription of multiple inflammatory genes and is a probable drug target.[14–16] Two probes, NF-D1 and NF-D2, were prepared to test quantitative detection of p50 binding to DNA. Their double-stranded regions are identical and include an NF-κB binding sequence, d(GGGACTTTCC). These probes interact with each other through their single-stranded tails and are then involved in a strand exchange reaction. Each strand of NF-D1 was labeled with 6FAM and DABCYL at the double-stranded terminus. NF-D1, various concentrations of recombinant p50, and NF-D2 were mixed in a half-area 96-well microplate and changes in fluorescence were measured. Time courses of these changes are shown in Figure 2. The fluorescence signal of NF-D1 increased rapidly within 30 min after addition of NF-D2 and was fivefold higher than that of NF-D1 alone at 60 min in the absence of p50. Fluorescence elevation was suppressed in a p50 concentration-dependent manner by half at 40 nM p50 and almost completely at 320 nM p50.

Duplex NF-01F02, which consists of NF-01F and NF-02, was prepared as a positive control as a completely exchanged product. Fluorescence of NF-01F02 was not affected by p50 (Fig. 2). We then optimized the concentrations of NF-D1 and

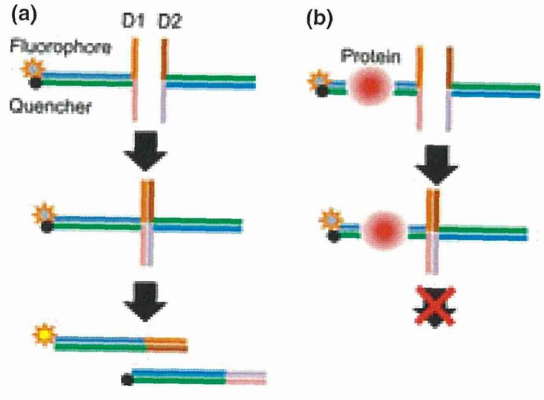

Fig. 1. Principles of the DSE-FRET assay. (a) In the absence of target protein, strand exchange between D1 and D2 will occur and fluorescence will be elevated. (b) In the presence of target protein, strand exchange will not occur and fluorescence will remain quenched.

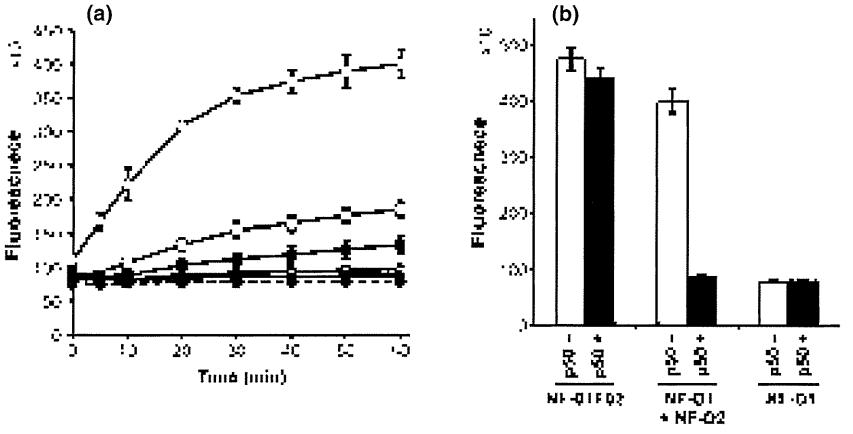

Fig. 2. Dose-dependent suppression of DNA strand exchange by p50. (a) Five microliters of 40 nM NF-D1 was mixed with 5 μL of 0 nM (open circles), 400 nM (open squares), 800 nM (closed squares), 1600 nM (open triangles), or 3200 nM (closed triangles) p50 and incubated for 30 min. Then, 40 μL of 10 nM NF-D2 was added and fluorescence was measured; thus, the final concentrations of p50 were 0, 40, 80, 160, and 320 nM, respectively. Closed circles with a dotted line represent NF-D1 alone. (b) Fluorescence at 60 min for a positive control completely exchanged product (NF-01F + NF-02, named NF-01F02), an exchanged product (NF-D1 + NF-D2), and an unexchanged product (NF-D1 alone) with 0 or 320 nM p50. Error bars represent ±3 SD (n = 4).

NF-D2. Varied concentrations of NF-1D (1, 2, and 4 nM) were mixed with twofold or fourfold amounts of NF-2D in the presence (40 nM) or absence of p50. As shown in Table 1, the combination of 2 nM NF-D1 and 8 nM NF-D1 showed the highest Z'-factor (0.93). S/B values (ratio in the absence to presence of p50) were 1.9–2.3 and were not influenced by the DNA concentration. Therefore, we used 2 nM NF-D1 with 8 nM NF-D2 in the following assays.

We examined the specificity of the assay by using double-stranded competitor DNA. NF-cpt1 is a specific competitor DNA bearing a NF-κB binding site. NF-cpt2, NF-cpt3, NF-cpt4, and NF-cpt5 are non-specific competitors with one to four nucleotides substituted in the NF-κB binding site. NF-cpt1 completely restored the fluorescence suppressed by p50 (Fig. 3). The restoration level decreased as the number of substituted nucleotides in non-specific competitors increased and NF-cpt5, with four substituted nucleotides, had little effect on p50 binding. For further evaluation of specificity, we prepared non-specific probes, NFs-D1 and NFs-D2, with nucleotide substitutions as in NF-cpt5. The fluorescence signal of the nonspecific probes was not affected by p50 (Fig. 3). Hence, we concluded that p50 suppressed strand exchange in a sequence-specific manner.

A 10-point dose–response experiment with Evans Blue (EB) was also carried out. One hundred μM Evans Blue inhibits NF-κB binding to DNA by EMSA and has been suggested to bind non-covalently to the p50 DNA binding region by molecular modeling.[17] In DSE-FRET, 10 μM EB showed little effect on p50, but 30 μM EB inhibited p50 completely (Fig. 4). Evans Blue also inhibited p52 in a similar fashion. The IC_{50} values of EB for p50 and p52 inhibition were 12.9 and 12.8 μM, respectively. We also showed that our method can be used for evaluation of an uncompetitive inhibitor, (−)-DHMEQ, which binds covalently to a specific Cys residue of Rel family proteins to inhibit their DNA binding.[18,19] We detected an inhibitory effect of (−)-DHMEQ on p50 and p52 by DSE-FRET (Fig. 5). As shown previously,[19] (−)-DHMEQ was less potent against p52 (IC_{50} 62.5 μM) compared to p50 (IC_{50} 8.8 μM).

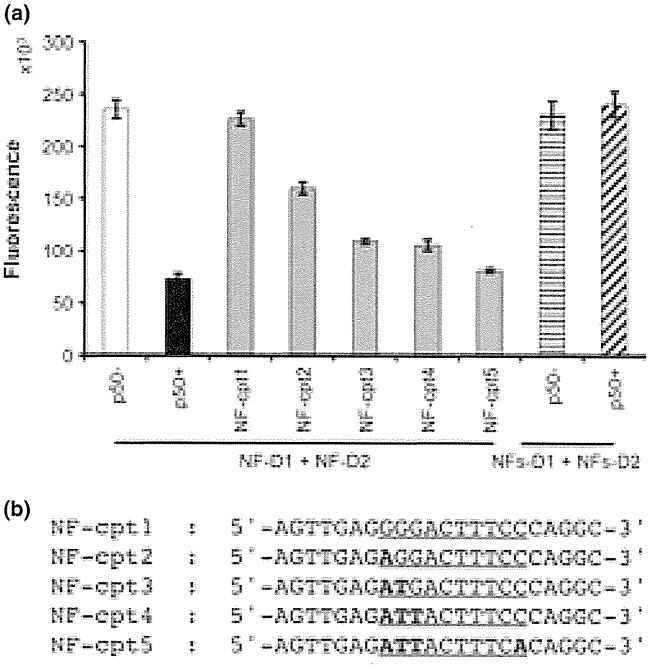

Fig. 3. Specificity of DSE-FRET. (a) 2.5 μL of 2000 nM competitor was mixed with 2.5 μL of 800 nM p50 and incubated for 30 min. Then, 5 μL of 20 nM NF-D1 was added and incubated for a further 30 min. Finally, 40 μL of 10 nM NF-D2 was added and fluorescence was measured: NF-D1 and NF-D2 without p50 (white bar), without competitor (black bar), and with competitors (gray bars). Horizontally and diagonally striped bars indicate non-specific probes (NFs-D1 + NFs-D2) without and with p50, respectively. (b) Sequences of the competitor upper strand are shown: underline, nuclear factor-κB (NF-κB) binding site; bold type, substituted nucleotide in binding site. Error bars represent ±3 SD (n = 4).

Table 1. Optimization of probe concentration

D1 (nM)	D2 (nM)	S/B	Z′-factor
4	8	1.9	0.77
2	4	2.3	0.90
2	8	2.2	0.93
1	2	2.1	0.83
1	8	1.9	0.82

Discussion

The DSE-FRET technique can detect protein–DNA interaction quantitatively and specifically using a simple procedure; just mix and measure. It detected p50 binding with a high Z'-factor and a dose–response analysis was carried out with two types of inhibitor (EB and (−)-DHMEQ). Moreover, the differential effect of (−)-DHMEQ on p50 and p52 was well displayed. Yamamoto *et al.* found that (−)-DHMEQ inhibited

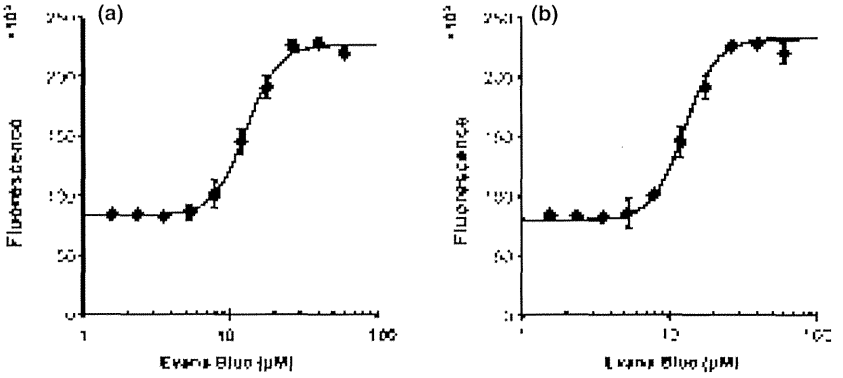

Fig. 4. Dose–response of Evans Blue (EB). Half a microliter of various concentrations of EB was mixed with 4.5 μL of 890 nM p50 (a) or p52 (b) and incubated for 30 min. Then, 5 μL of 20 nM NF-D1 was added and incubated for a further 30 min. Finally, 40 μL of 10 nM NF-D2 was added and fluorescence was measured. Horizontal axes show the concentration of EB in incubations with protein and NF-D1. Error bars represent ±SD (n = 4).

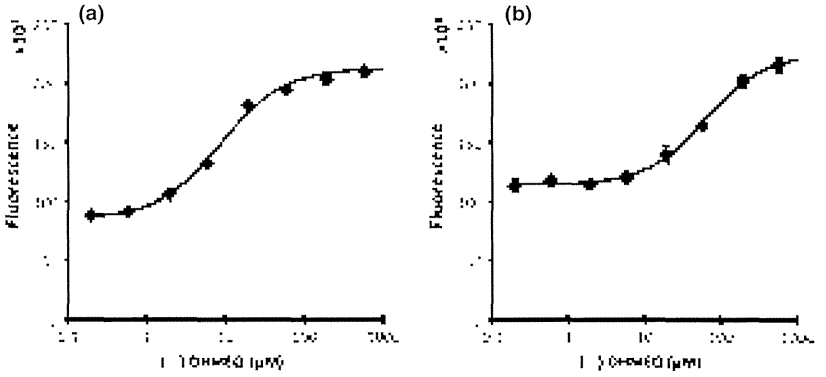

Fig. 5. Dose–response of dehydroxymethylepoxyquinomicin ([−]-DHMEQ). Half a microliter of various concentrations of (−)-DHMEQ was mixed with 4.5 μL of 440 nM p50 (a) or p52 (b) and incubated for 30 min. Then, 5 μL of 20 nM NF-D1 was added and incubated for a further 30 min. Finally, 40 μL of 10 nM NF-D2 was added and fluorescence was measured. Horizontal axes show the concentrations of (−)-DHMEQ in incubations with protein and NF-D1. Error bars represent ±SD (n = 4).

p50 more strongly than p52 in EMSA analysis.[19] The same preference of the inhibitor was shown by DSE-FRET, with the IC_{50} for inhibition of p50 being sevenfold lower than that for p52. However, the amount of (−)-DHMEQ required to inhibit the proteins differed between the two methods. A (−)-DHMEQ concentration fourfold that of p50 (80–20 μM) inhibited protein binding completely in EMSA,[19] whereas a (−)-DHMEQ concentration 44-fold that of p50 (8.8–0.2 μM) was required to inhibit half of the p50 binding in DSE-FRET. In contrast, inhibition of (−)-DHMEQ to p52 was shown only by DSE-FRET. The basis for these differences is unclear.

As a stable and homogeneous assay, DSE-FRET is particularly useful for high throughput screening. These features are particularly important for initial screening of a huge combinatorial library. Although we carried out the assay in a 96-well (half area) format, a 384-well format can be used with appropriate specialized equipment. The probes used in DSE-FRET consist of a double-stranded moiety and two single-stranded tails. Inadequate intra- and intermolecular hybridization of tails interferes with appropriate formation of a four-way junction and markedly reduces the efficiency of strand exchange. Thus, we evaluated 13 tails before choosing the tails used here. These tails were also confirmed to not have protein binding sequences using the transcription factor analysis tool TFSearch (version 1.3 online, http://mbs.cbrc.jp/research/db/TFSEARCH.html). Therefore, these tails may be applicable universally. The double-stranded moiety should have a sequence that allows protein binding, but is otherwise not restricted in sequence. Taken together, these features make design of a probe for DSE-FRET as easy as that for EMSA.

To our knowledge, this is the first report to show that NF-κB blocks spontaneous strand exchange. Several proteins, including histone octamer, p53, TRF1, and TRF2, have also been found to block strand exchange.[10–12] However, this blockage can be explained based on particular features of these proteins: thus, the histone octamer forms a large protein–DNA complex and the other proteins have junction-binding activity. Panyutin and Hsieh[20] found that spontaneous strand exchange is also blocked by a mismatch, which suggests that this process may be blocked easily by a small energy barrier.

In this paper, we established a novel technique to identify NF-κB inhibitors as anticancer drugs. Nuclear factor-κB is a desirable target for therapy in various cancers and inflammatory diseases.[21,22] In most cancer cells, NF-κB is localized in the nucleus and is constitutively active. This persistent activity of nuclear NF-κB protects cancer cells from apoptotic cell death. Therefore, anticancer drug targeting of NF-κB may have great therapeutic value by inhibiting cell growth or increasing the sensitivity of conventional chemotherapy. We believe that the DSE-FRET assay will be a powerful tool to isolate novel NF-κB inhibitors that inhibit DNA binding activity and cancer growth. We also found that DNA binding of transcription factors SP1 and AP1 (c-jun) can be detected by DSE-FRET (data not shown). Therefore, DSE-FRET may be applicable to detection of many DNA-binding proteins.

Acknowledgment

This study was carried out as part of the Project for Development of Innovative Research on Cancer Therapeutics (P-Direct), Ministry of Education, Culture, Sports, Science and Technology of Japan.

Disclosure Statement

H.T. owns stock in MiRTeL Inc. The other authors have no conflict of interest.

References

1 Latchman DS. Transcription factors as potential targets for therapeutic drugs. *Curr Pharm Biotechnol* 2000; **1**: 57–61.
2 Darnell JE Jr. Transcription factors as targets for cancer therapy. *Nat Rev Cancer* 2002; **2**: 740–9.
3 Garner MM, Revzin A. A gel electrophoresis method for quantifying the binding of proteins to specific DNA regions: application to components of the Escherichia coli lactose operon regulatory system. *Nucleic Acids Res* 1981; **9**: 3047–60.
4 Fried M, Crothers DM. Equilibria and kinetics of lac repressor-operator interactions by polyacrylamide gel electrophoresis. *Nucleic Acids Res* 1981; **9**: 6505–25.
5 Galas DJ, Schmitz A. DNAse footprinting: a simple method for the detection of protein-DNA binding specificity. *Nucleic Acids Res* 1978; **5**: 3157–70.
6 Gubler ML, Abarzúa P. Nonradioactive assay for sequence-specific DNA binding proteins. *Biotechniques* 1995; **18**: 1008, 1011–4.
7 Heyduk T, Heyduk E. Molecular beacons for detecting DNA binding proteins. *Nat Biotechnol* 2002; **20**: 171–6.
8 Wang J, Li T, Guo X, Lu Z. Exonuclease III protection assay with FRET probe for detecting DNA-binding proteins. *Nucleic Acids Res* 2005; **33**: e23.
9 Chen Z, Ji M, Hou P, Lu Z. Exo-dye-based assay for rapid, inexpensive, and sensitive detection of DNA-binding proteins. *Biochem Biophys Res Commun* 2006; **345**: 1254–63.
10 Grigoriev M, Hsieh P. A histone octamer blocks branch migration of a Holliday junction. *Mol Cell Biol* 1997; **17**: 7139–50.
11 Prabhu VP, Simons AM, Iwasaki H, Gai D, Simmons DT, Chen J. p53 blocks RuvAB promoted branch migration and modulates resolution of Holliday junctions by RuvC. *J Mol Biol* 2002; **316**: 1023–32.
12 Poulet A, Buisson R, Faivre-Moskalenko C *et al.* TRF2 promotes, remodels and protects telomeric Holliday junctions. *EMBO J* 2009; **28**: 641–51.
13 Takeiri M, Horie K, Takahashi D *et al.* Involvement of DNA binding domain in the cellular stability and importin affinity of NF-κB component RelB. *Org Biomol Chem* 2012; **10**: 3053–9.
14 May MJ, Ghosh S. Signal transduction through NF-kappa B. *Immunol Today* 1998; **19**: 80–8.
15 Sha WC. Regulation of immune responses by NF-kappa B/Rel transcription factor. *J Exp Med* 1998; **187**: 143–6.
16 Barnes PJ, Karin M. Nuclear factor-kappaB: a pivotal transcription factor in chronic inflammatory diseases. *N Engl J Med* 1997; **336**: 1066–71.
17 Sharma RK, Otsuka M, Pande V, Inoue J, João Ramos M. Evans Blue is an inhibitor of nuclear factor-kappaB (NF-kappaB)-DNA binding. *Bioorg Med Chem Lett* 2004; **14**: 6123–7.
18 Umezawa K. Possible role of peritoneal NF-κB in peripheral inflammation and cancer: lessons from the inhibitor DHMEQ. *Biomed Pharmacother* 2011; **65**: 252–9.
19 Yamamoto M, Horie R, Takeiri M, Kozawa I, Umezawa K. Inactivation of NF-kappaB components by covalent binding of (-)-dehydroxymethylepoxyquinomicin to specific cysteine residues. *J Med Chem* 2008; **51**: 5780–8.
20 Panyutin IG, Hsieh P. Formation of a single base mismatch impedes spontaneous DNA branch migration. *J Mol Biol* 1993; **230**: 413–24.
21 Karin M. NF-kappaB as a critical link between inflammation and cancer. *Cold Spring Harb Perspect Biol* 2009; **1**: a000141.
22 Baud V, Karin M. Is NF-kappaB a good target for cancer therapy? Hopes and pitfalls. *Nat Rev Drug Discov* 2009; **8**: 33–40.

OPEN ACCESS Freely available online

PLOS | ONE

Reprogramming Suppresses Premature Senescence Phenotypes of Werner Syndrome Cells and Maintains Chromosomal Stability over Long-Term Culture

Akira Shimamoto[1]*, Harunobu Kagawa[1], Kazumasa Zensho[1], Yukihiro Sera[1], Yasuhiro Kazuki[2], Mitsuhiko Osaki[2,3], Mitsuo Oshimura[2], Yasuhito Ishigaki[4], Kanya Hamasaki[5], Yoshiaki Kodama[5], Shinsuke Yuasa[6], Keiichi Fukuda[6], Kyotaro Hirashima[7], Hiroyuki Seimiya[7], Hirofumi Koyama[8], Takahiko Shimizu[8], Minoru Takemoto[9], Koutaro Yokote[9], Makoto Goto[10], Hidetoshi Tahara[1]*

1 Department of Cellular and Molecular Biology, Graduate School of Biomedical & Health Sciences, Hiroshima University, Hiroshima, Japan, **2** Department of Biomedical Science, Institute of Regenerative Medicine and Biofunction, Graduate School of Medical Science, Tottori University, Yonago, Japan, **3** Division of Pathological Biochemistry, Faculty of Medicine, Tottori University, Yonago, Japan, **4** Medical Research Institute, Kanazawa Medical University, Kahoku, Ishikawa, Japan, **5** Department of Genetics, Radiation Effects Research Foundation, Hiroshima, Japan, **6** Department of Cardiology, Keio University School of Medicine, Tokyo, Japan, **7** Division of Molecular Biotherapy, The Cancer Chemotherapy Center, Japanese Foundation For Cancer Research, Tokyo, Japan, **8** Department of Advanced Aging Medicine, Chiba University Graduate School of Medicine, Chiba, Japan, **9** Department of Clinical Cell Biology and Medicine, Chiba University Graduate School of Medicine, Chiba, Japan, **10** Division of Orthopedic Surgery & Rheumatology, Tokyo Women's Medical University Medical Center East, Tokyo, Japan

Abstract

Werner syndrome (WS) is a premature aging disorder characterized by chromosomal instability and cancer predisposition. Mutations in *WRN* are responsible for the disease and cause telomere dysfunction, resulting in accelerated aging. Recent studies have revealed that cells from WS patients can be successfully reprogrammed into induced pluripotent stem cells (iPSCs). In the present study, we describe the effects of long-term culture on WS iPSCs, which acquired and maintained infinite proliferative potential for self-renewal over 2 years. After long-term cultures, WS iPSCs exhibited stable undifferentiated states and differentiation capacity, and premature upregulation of senescence-associated genes in WS cells was completely suppressed in WS iPSCs despite *WRN* deficiency. WS iPSCs also showed recapitulation of the phenotypes during differentiation. Furthermore, karyotype analysis indicated that WS iPSCs were stable, and half of the descendant clones had chromosomal profiles that were similar to those of parental cells. These unexpected properties might be achieved by induced expression of endogenous telomerase gene during reprogramming, which trigger telomerase reactivation leading to suppression of both replicative senescence and telomere dysfunction in WS cells. These findings demonstrated that reprogramming suppressed premature senescence phenotypes in WS cells and WS iPSCs could lead to chromosomal stability over the long term. WS iPSCs will provide opportunities to identify affected lineages in WS and to develop a new strategy for the treatment of WS.

Citation: Shimamoto A, Kagawa H, Zensho K, Sera Y, Kazuki Y, et al. (2014) Reprogramming Suppresses Premature Senescence Phenotypes of Werner Syndrome Cells and Maintains Chromosomal Stability over Long-Term Culture. PLoS ONE 9(11): e112900. doi:10.1371/journal.pone.0112900

Editor: Zhongjun Zhou, The University of Hong Kong, Hong Kong

Received August 9, 2014; **Accepted** October 16, 2014; **Published** November 12, 2014

Data Availability: The authors confirm that all data underlying the findings are fully available without restriction. The microarray dataset are available from the NCBI Gene Expression Omnibus database (accession number GSE62114).

Funding: This work was supported by a Grant-in-Aid for Challenging Exploratory Research No. 25670030 (to A.S) and for Scientific Research No. 20014015 (to H.T) and No. 24590902 (to M.G) from the Ministry of Education, Culture, Sports, Science and Technology of Japan. This work was also supported by a Health and Labor Sciences Research Grant from the Ministry of Health Labor and Welfare of Japan (to A.S). The funders had no role in study design, data collection and analysis, decision to publish, or preparation of the manuscript.

Competing Interests: The authors have declared that no competing interests exist.

* Email: shim@hiroshima-u.ac.jp (AS); toshi@hiroshima-u.ac.jp (HT)

Introduction

Werner syndrome (WS) is a rare human autosomal recessive disorder characterized by early onset of aging-associated diseases, chromosomal instability, and cancer predisposition [1,2]. Fibroblasts from WS patients exhibit premature replicative senescence [3], and *WRN*, a gene responsible for the disease, encodes a RecQ-type DNA helicase [4–7], that is involved in maintenance of chromosome integrity during DNA replication, repair, and recombination [8,9]. WRN helicase is known to interact with a variety of proteins associated with DNA metabolism including proteins of replication fork progression, base excision repair, and telomere maintenance [8,9]. The dysfunction of WRN helicase causes defects in telomeric lagging-strand synthesis and telomere loss during DNA replication [10]. Further, it is also reported that telomere loss caused by a defect in WRN helicase involves chromosome end fusions that are suppressed by telomerase [11]. These observations suggest that premature senescence in WS cells reflects defects in telomeric lagging-strand synthesis followed by accelerated telomere loss during DNA replication.

Somatic cell reprogramming follows the introduction of several pluripotency genes including Oct3/4, Sox2, Klf4, c-myc, Nanog

and Lin-28 into differentiated cells such as dermal fibroblasts, blood cells, and other cell types [12–17]. During reprogramming, somatic cell-specific genes are suppressed, and embryonic stem cell (ESC)-specific pluripotency genes are induced, leading to the generation of iPSCs with undifferentiated states and pluripotency [18]. In addition, ESC-like infinite proliferative potential is directed by induction of the endogenous telomere reverse-transcriptase catalytic subunit (hTERT) gene and the reactivation of telomerase activity during reprogramming [13,18].

Recently, Cheung et al. demonstrated that cells from WS patients were successfully reprogrammed into iPSCs with restored telomere function, suggesting that the induction of hTERT during reprogramming suppresses telomere dysfunction in WS cells lacking *WRN* [19]. However, the effects of long-term culture on the undifferentiated states, self-renewal abilities, and differentiation potentials of WS iPSCs remain unknown. In a previous study, progressive telomere shortening and loss of self-renewal ability were observed in iPSCs from dyskeratosis congenital patient cells in a long-term culture [20], warranting the evaluation of the properties of patient cell-derived iPSCs with telomere dysfunctions over the long term.

In this study, we cultured WS iPSCs with self-renewal capacity and infinite proliferative potential for over 2 years and reported similar properties to those of normal iPSCs including undifferentiated states and differentiation ability. Notably, WS iPSCs maintained stable karyotypes and their potential to recapitulate premature senescence phenotypes during differentiation over the long term. The present data demonstrate that reprogramming suppresses premature senescence phenotypes in WS cells by reversing the aging process and restoring telomere maintenance over the long term.

Materials and Methods

Cell lines

WS patients were diagnosed on the basis of clinical symptoms and *WRN* gene mutations. A0031 WS patient fibroblasts from a 37-year-old male were obtained from Goto Collection of RIKEN Bioresource Center (https://www.brc.riken.jp/lab/cell/english/index_gmc.shtml) [21], and WSCU01 patient fibroblasts were isolated from a 63-year-old Japanese male who was diagnosed at Chiba University. Both fibroblast isolates had type 4/6 heterozygous mutations. TIG-3 human fetal lung-derived fibroblast cells and WS patient-derived fibroblasts were used to generate iPSC lines. PLAT-A cells (kindly provided from Dr. Toshio Kitamura) were used to produce retroviruses [22]. SNL 76/7 (SNL) cells (DS pharma biomedical) were used as feeder layers for reprogramming of fibroblasts and maintenance of iPSCs. The human fibroblast-derived iPSC line iPS-TIG114-4f1 was obtained from the National Institute of Biomedical Innovation [23].

PLAT-A cells, TIG-3 fibroblasts, TIG-114 fibroblasts from the 36-year-old male, and SNL cells were grown in the Dulbecco's modified Eagle's medium (DMEM; Sigma) supplemented with 10% fetal bovine serum (FBS; Hyclone) and antibiotics (Invitrogen). WS fibroblasts were maintained on collagen-coated dishes (Nitta Gelatin), SNL cells were maintained on gelatin-coated dishes (Nitta Gelatin), and iPSCs were maintained in the ES medium comprising Knockout DMEM (Invitrogen) supplemented with 20% Knockout Serum Replacement (Invitrogen), glutamine, non-essential amino acids, β-mercaptoethanol and 4-ng/ml basic FGF. All cells were maintained at 37°C under 5% CO_2 atmosphere.

Generation of iPSCs

The generation of iPSCs was performed as described previously [13]. Briefly, 2×10^6 PLAT-A cells were plated in T25 flasks (Biocoat, BD Falcon), and were transfected with 4 μg pMXs-OCT3/4, SOX2, KLF-4, and c-myc (Addgene) 1 day later. Twenty-four hours after transfection, the culture medium was replaced with a fresh medium and cells were incubated for 24 h prior to harvest of viral supernatants. Viral supernatants containing Yamanaka factors were combined in even ratios.

For reprogramming experiments, 3×10^5 fibroblasts were seeded on 60-mm dishes and were infected with viral supernatants containing Yamanaka factors in the presence of 8 μg/ml polybrene 1 day later. Four days after infection, fibroblasts were harvested, and 1×10^5 cells were reseeded onto mitomycin C-inactivated SNL feeder layers on 100-mm dishes. Twenty-four hours after reseeding, the medium was replaced with the ES medium, and cultures were maintained by replacing the medium every other day. Approximately 30 days after retroviral transduction, emerging iPSC colonies with ESC colony-like flat and round shapes were picked up by mechanical dissection and were plated onto fresh feeder layers on 4-well plates (Thermo Scientific Nunc). Subsequently, iPSC lines were established by successive passages onto fresh feeder layers with split ratios between 1:3 and 1:5 using dispase (Roche Applied Science).

Alkaline phosphatase activity

Undifferentiated states of emerging colonies were examined using alkaline phosphatase staining. After formalin fixation, colonies were stained with reaction buffer containing 100 mM Tris-Cl (pH 8.5), 0.25 mg/ml Naphthol AS-BI phosphate (Sigma) and 0.25 mg/ml fast red violet LB salt (Sigma).

Embryoid body formation and in vitro differentiation

Clumps of iPSCs were transferred to non-adherent polystyrene dishes containing the ES medium without basic FGF to form embryoid bodies (EBs). The medium was replaced every other day. After 8 days of floating culture, EBs were transferred onto gelatin-coated plates and were maintained in DMEM supplemented with 10% FBS, β-mercaptoethanol, and antibiotics for another 8 days. For detection of senescence phenotypes during differentiation, Y-27632-treated iPSCs were dissociated into single cell suspensions with Accutase (Innovative Cell Technologies) and 1×10^4 cells were transferred into 96-well V-shaped bottom plates (Greiner Bio-One) to form evenly sized EBs. After 12 days of EB formation in the ES medium without basic FGF, EBs were cultured in DMEM supplemented with 10% FBS, β-mercaptoethanol, and antibiotics.

Teratoma formation

After harvest, 1×10^6 iPSCs were injected into the testes of a severe combined immunodeficient (SCID) mice (CREA, Japan). Three months after injection, tumors were dissected and were fixed using 4% paraformaldehyde. Subsequently, dissected tumor tissues were embedded in paraffin and were sliced and stained with hematoxylin and eosin.

Western blot

Whole cell lysates were prepared in SDS sample buffer and subjected to electrophoresis on 8% SDS-polyacrylamide gels, and separated proteins were transferred onto PVDF membranes (FluoroTrans W, Pall Corporation). Membranes were blocked with TBS-T containing 5% skim milk and were then incubated with anti-WRN (1:500, 4H12, Abcom) or anti-β-actin (1:30000,

Ac-15, Sigma) monoclonal antibodies for 3 h at room temperature. Membranes were then washed with TBS-T and were incubated with horseradish peroxidase-conjugated anti-mouse IgG (1:5000, NA931V, GE) for 1 h at room temperature. Chemiluminescence reactions were performed using Western Lightning Plus-ECL (PerkinElmer) and were detected using exposure of x-ray films.

Mutation analysis

The DNA fragments mut.4 (c.3139-1G>C) and mut.6 (c.1105C>T) were amplified with the primer pairs WS_mut4_U, GGTAAACGGTGTAGGAGTCTGC and WS_mut4_L, CTTGTGAGAGGCCTATAAACTGG, and WS_mut6_U, TGAAGATTCAACTACTGGGGGAGTAC and WS_ mut6_L, ACGGGAATAAAGTCTGCCAGAACC, respectively, using genomic DNA as a template. Mutations were analyzed by direct sequencing using these PCR primers.

Short tandem repeat (STR) analysis

Genomic DNAs were purified from WS fibroblasts and their derivative iPSC clones using phenol/chloroform extraction and were then used for analysis using a Cell ID System (Promega). PCR products were analyzed using an Applied Biosystems 3130xl Genetic Analyzer and GeneMapper software.

Gene expression profiling

Cy3-labeled total RNAs were hybridized onto Human Genome U133 Plus 2.0 Arrays (GeneChip, Affymetrix). Arrays were then scanned using the GeneChip Scanner 3000 7G (Affymetrix), and the obtained data were analyzed by Affymetrix Expression Console Software. The microarray dataset has been deposited in the NCBI Gene Expression Omnibus database under Series Accession GSE62114.

Measurement of telomere length

Genomic DNAs were digested using *Hinf*I restriction enzyme (TakaraBio), and were subjected to electrophoresis on 1% agarose gels. Size-fractionated DNAs were transferred onto Hybond-N+ membranes (GE). Membranes were hybridized with a digoxigenin-labeled $(CCCTAA)_4$ probe, and TRFs were detected using TeloTAGGG Telomere Length Assays (Roche Applied Science) according to the manufacturer's instructions.

RT-PCR and real-time qRT-PCR analysis of mRNA expression

Total RNA was prepared using RNeasy spin columns (Qiagen) according to the manufacturer's instructions. RT-PCR was performed with 0.1 μg of total RNA using SuperScript One-Step RT-PCR (Invitrogen). Semi-quantitative analysis was performed after converting total RNA into cDNA using a High Capacity RNA-to-cDNA kit (Life Technologies), and real-time PCR was performed using a Rotor-Gene SYBR Green PCR kit (Qiagen). Relative gene expression levels were analyzed according to the ΔΔCt method using Ct values of GAPDH mRNA as an internal control. Primer sequences are listed in Tables S1 and S2.

Immunofluorescence cytochemistry

Following fixation of iPSCs and differentiated cells with 4% paraformaldehyde for 15 min at 4°C, cells were permeabilized with 0.1% Triton X-100, washed with PBS containing 2% BSA, and incubated with primary antibodies diluted in PBS containing 2% BSA.

Primary antibodies against Nanog (1:200, Cell Signaling, D73G4), SSEA-4 (1:200, Cell Signaling, MC813), Tra-1-60 (1:200, Cell Signaling, #4746), Tra-1-81 (1:200, Cell Signaling, #4745), βIII-tubulin (1:200, Millipore, TU-20), desmin (1:200, Neomarkers, RB-9014-P0), vimentin (1:200, Santa Cruz, V9), and α-fetoprotein (1:500, Sigma, HPA010607) were detected using the secondary antibodies Alexa 488-conjugated anti-goat IgG (1:500, Invitrogen, A11055), Alexa 488-conjugated anti-mouse IgG (1:500, Invitrogen, A11001), Alexa 488-conjugated anti-mouse IgM (1:500, Invitrogen, A21042), and Alexa 488-conjugated anti-rabbit IgG (1:500, Invitrogen, A11013). Cell nuclei were stained with 1- μg/ml 4',6-diamidino-2-phenylindole (DAPI).

Karyotype analysis

After culturing iPSCs in the ES medium containing 100-ng/ml colcemid for 5 h at 37°C, cells were harvested using trypsin and were treated with 0.075 M KCl for 15 min at 37°C. Cells were then fixed in Carnoy's fluid, and chromosome slides were prepared. G-banding analysis was conducted using a previously described method [24].

M-FISH was performed with the Multi-color probe kit "24XCyte" (MetaSystems, Altlussheim, Germany) according to the manufacturer's protocol with slight modifications. Briefly, probes were denatured at 75°C for 5 min and were hybridized to metaphase spreads, which were denatured in 0.07 N NaOH at room temperature for 1 min. Slides were then incubated at 37°C for 2 nights and were then washed in 0.4× SSC at 72°C for 2 min, in 2× SSC containing 0.05% Tween 20 at room temperature for 30 s, and in 2× SSC at room temperature for 1 min, and the mounting medium (DAPI, 125 ng/ml) and a cover slip were applied. Acquisition and analysis of M-FISH images were performed using a CytoVision ChromoFluor System (Applied Imaging, Newcastle upon Tyne, UK).

Transduction of hTERT gene

PT67 retrovirus packaging cells (Takara Bio USA, Madison, WI, USA) were transfected with pMSCV-hTERT-puro using GenePorter II according to the manufacturer's protocol. After 24 h, the culture medium was replaced, cells were incubated for a further 24 h period, and viral supernatants were harvested, A0031 and WSCU01 WS fibroblasts were infected with viral supernatant in the presence of 8 μg/ml polybrene. Confluent infected cells were then split into 2 new dishes, and puromycin selection of infected cells was initiated at the following passage. Confluent infected cells were then passaged in 4-fold dilutions, leading to an increase in 2 population doubling levels for each passage.

SA-β-gal assay

SA-β-gal staining was performed as described by Debacq-Chainiaux et al. [25].

Ethical statement

This study was approved by the Ethics Review Board of the Graduate School of Medicine, Chiba University and was conducted in accordance with the Declaration of Helsinki. Written informed consents were obtained from patients prior to tissue harvesting and iPSC generation, and patients were entitled to the protection of confidential information. Genome/gene analyses performed in this study were approved by the Ethics Committee for Human Genome/Gene Analysis Research at Hiroshima University. All animal experiments were performed in strict compliance with the protocol approved by the Institutional Animal Care and Use Committee of Tottori University (13-Y-

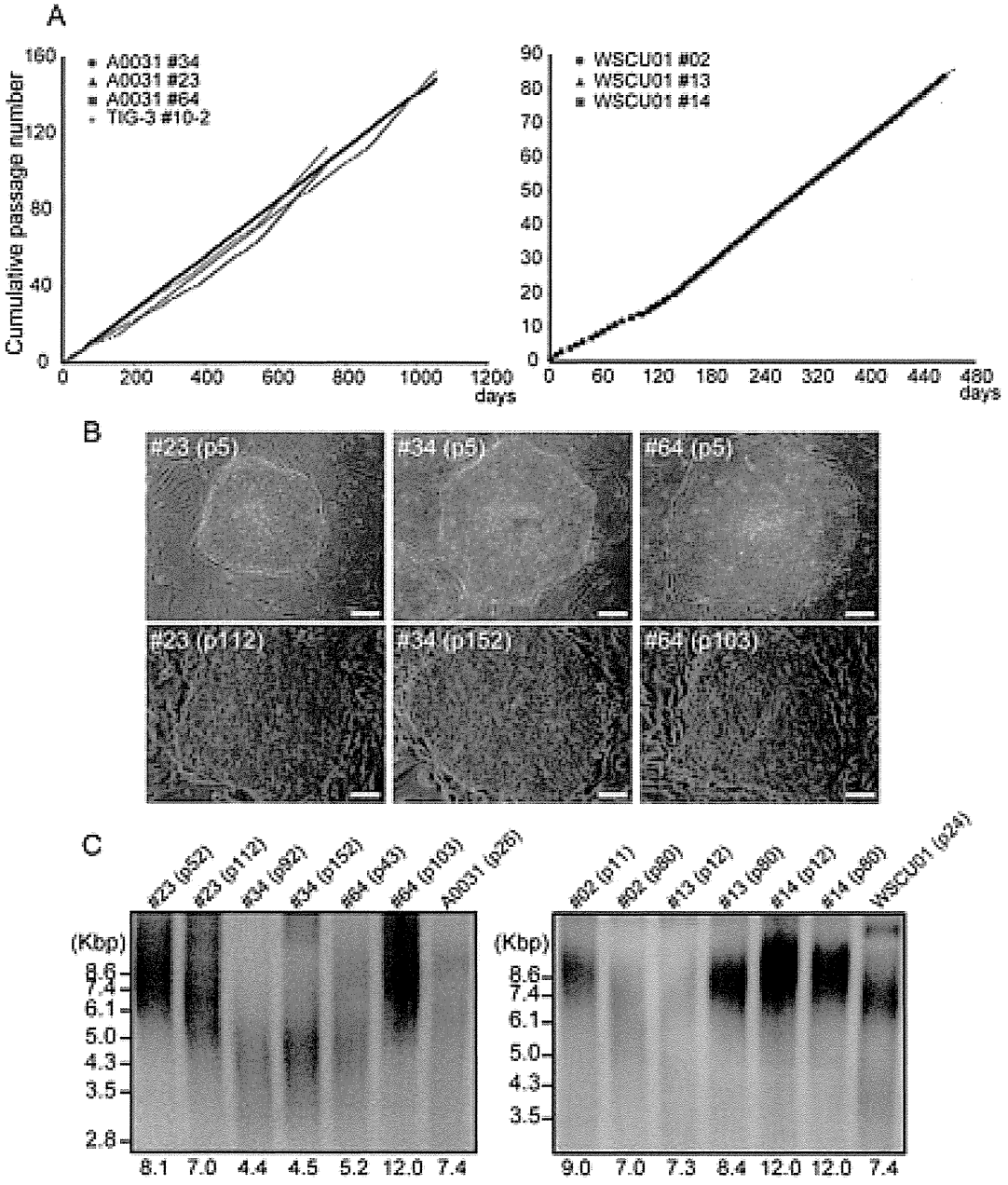

Figure 1. Infinite Proliferation of WS iPSCs after Long-Term Culture. (A) Cumulative passage number for WS iPSCs. (B) Colony morphologies of A0031-derived WS iPSC clones in early and late passages. Bars = 100 μm. (C) TRF length analysis of WS iPSC clones in early and late passages.
doi:10.1371/journal.pone.0112900.g001

18), and the Animal Care and Use Committee of Chiba University (25–131). All recombinant DNA experiments were performed in strict conformance with the guidelines of the Institutional Recombinant DNA Experiment Safety Committee at Hiroshima University.

Results

Infinite proliferative potential of WS iPSCs after long-term culture

To determine whether reprogramming provides WS cells with infinite proliferative potential, we generated iPSCs from WS patient fibroblasts. Morphologically distinct colonies from parental cells emerged after transduction of Yamanaka factors using retroviruses and showed elevated alkaline phosphatase activity (Figures S1A and S1B). Colonies were picked up, and 6 WS iPSC lines were established using fibroblasts from 2 independent WS patients after several passages. In western blotting analysis using an anti-WRN antibody, WRN protein was not detected in WS iPSCs but was expressed in both normal fibroblasts and iPSCs (Figure S2A). Direct sequencing analysis of WS iPSCs identified compound heterozygous Mut4/Mut6 mutations in the *WRN* gene similar to those observed in parental cells, and the derivation of WS iPSCs from parental cells was confirmed by STR analysis (Figures S2B and S2C). Finally, the 6 WS iPSC lines #23, #34, and #64 from A0031 and #02, #13, and#14 from WSCU01 were successfully established.

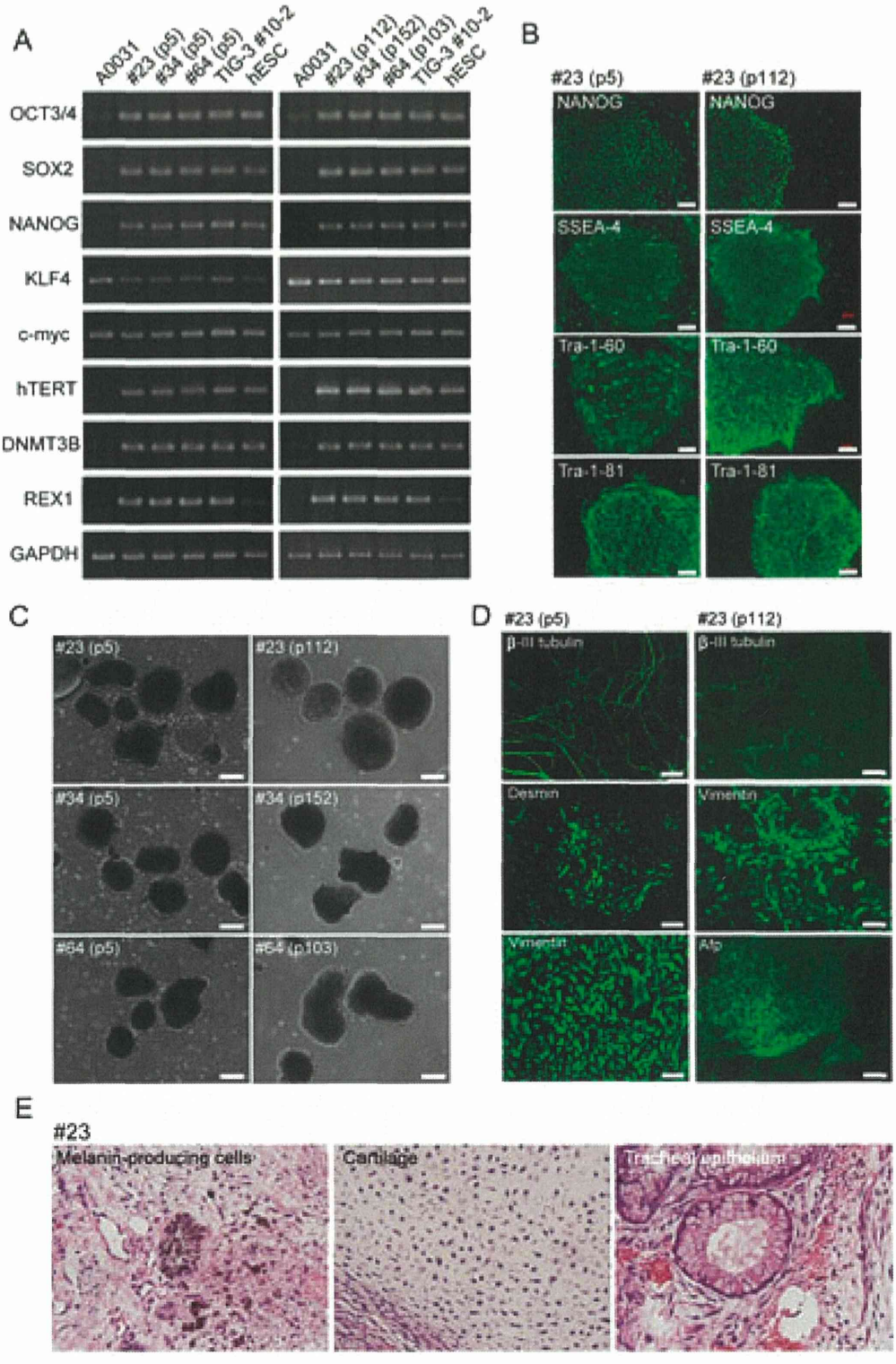

Figure 2. Sustained ESC-like characteristics of WS iPSCs after Long-Term Culture. (A) Expression of pluripotency genes in A0031-derived WS iPSC clones in early and late passages. (B) Expression of hESC markers in A0031-derived WS iPSC clone #23 in early and late passages. Bars = 100 μm. (C) EB formation in A0031-derived WS iPSC clones from early and late passages. Bars = 100 μm. (D) Immunocytochemical analysis of differentiation of EBs into 3 germ layers for A0031-derived iPSC clone #23 in early and late passages. β-III tubulin (ectoderm), desmin (mesoderm), vimentin (mesoderm and parietal endoderm), and α-fetoprotein (Afp, endoderm). Bars = 100 μm. (E) Hematoxylin and eosin histology of teratomas from A0031-derived iPSC clone #23. Formation of all 3 germ layers is shown including melanin-producing cells (ectoderm), cartilage (mesoderm), and tracheal epithelium (endoderm).
doi:10.1371/journal.pone.0112900.g002

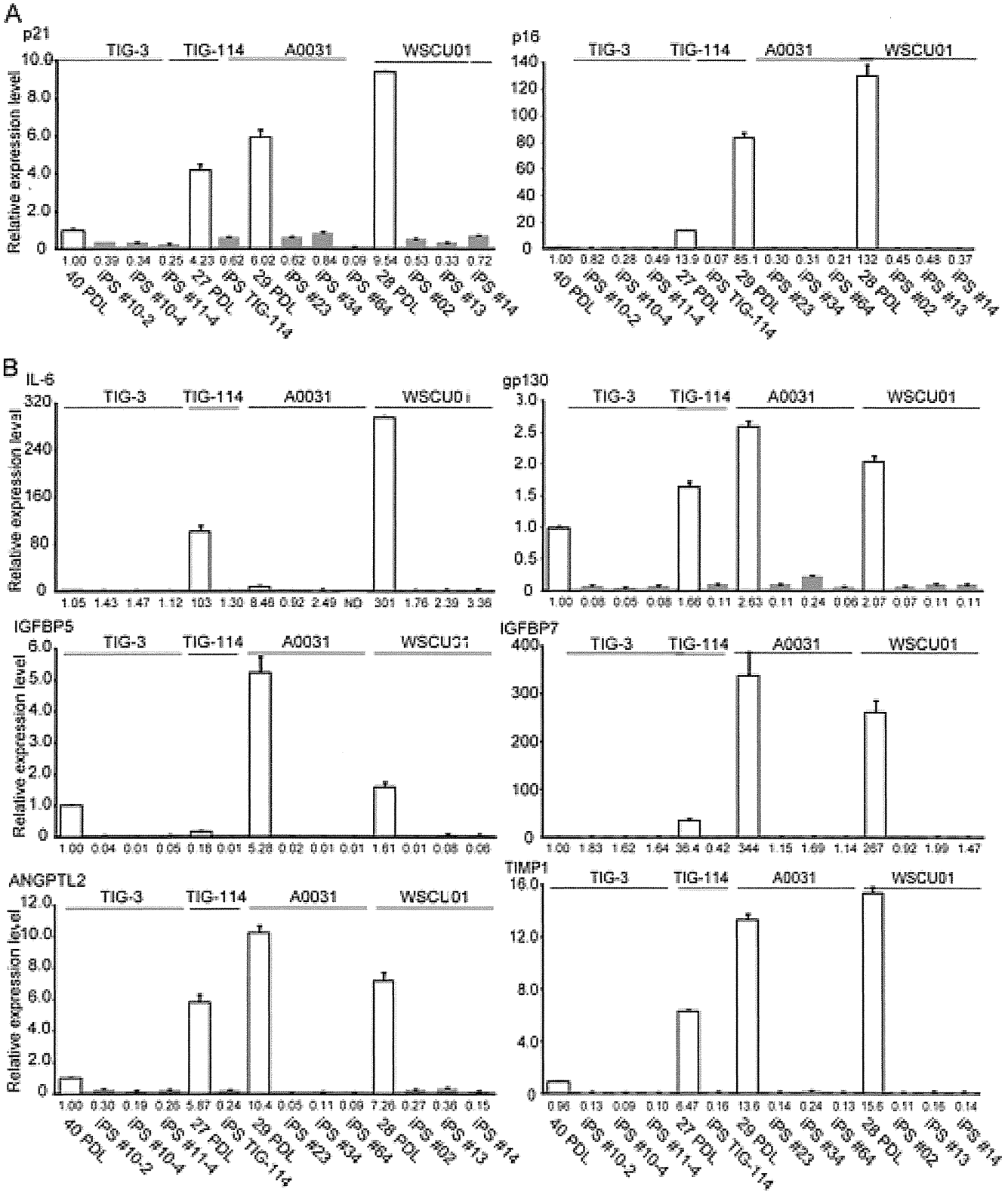

Figure 3. Suppression of Senescence-Associated Gene Expression in Reprogrammed WS iPSCs. (A) Expression of CDKI genes in parental fibroblasts and iPSCs. White columns show relative expression levels in the parental fibroblasts TIG-3, TIG-114, A0031, and WSCU01, and gray columns show those of their derived iPSC clones. Numbers under the horizontal axis in each graph show relative values in mRNA expression compared with that in TIG-3 fibroblasts. Values represent means of three technical replicates ± SD. (B) Expression of SASP genes in parental fibroblasts and iPSCs. Each graph is shown as in (A).
doi:10.1371/journal.pone.0112900.g003

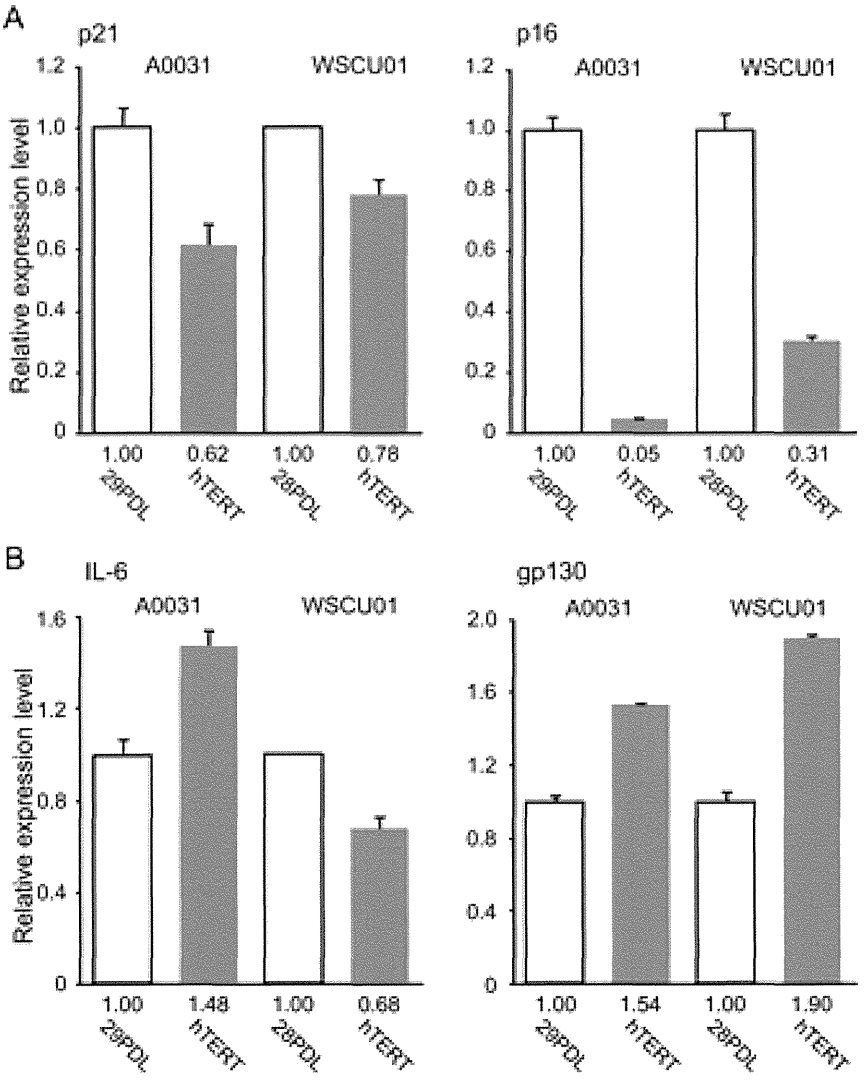

Figure 4. Reprogramming of the SASP gene loci is mediated by factors other than activated telomerase. (A) Expression of CDKI genes in WS fibroblasts and their hTERT-transduced derivatives. White columns show relative expression levels in A0031 and WSCU01 fibroblasts, and gray columns show those of their hTERT-transduced derivatives. Numbers under the horizontal axis in each graph show relative values in mRNA expression compared with that in parental fibroblasts. Values represent means of three technical replicates ± SD. (B) Expression levels of SASP genes in WS fibroblasts and their hTERT-transduced derivatives. Each graph is shown as in (C).
doi:10.1371/journal.pone.0112900.g004

WS iPSC lines from A0031 were cultured for 120 continuous passages over 2 years without morphological changes or loss of growth capacity (Figures 1A and 1B). Moreover, iPSC lines from WSCU01 proliferated for a year (Figures 1A and S1C). Average terminal restriction fragment (TRF) lengths in clones #23, #34, and #64 (A0031) were decreased, invariable, and increased during long-term culture, respectively, and similar telomere dynamics were observed in WSCU01-derived iPSC clones (Figure 1C).

Sustained ESC-like characters of WS iPSCs after long-term culture

To determine the persistence of ESC-like characteristics in WS iPSCs, we compared undifferentiated states and differentiation potentials between WS iPSCs from early and late passages. WS iPSC lines expressed pluripotency genes and hESC-specific surface markers during early passages (around p10), and during late passages (around p100; Figures 2A, 2B, S3 and S4). These iPSC lines also showed sustained formation of embryoid bodies and differentiation into 3 germ layers (Figures 2C, 2D, and S5). Furthermore, at around p50, WS iPSC lines generated teratomas that contained tissue structures of all 3 germ layers. These were consistent with those shown in normal iPSC lines after transplantation into the testes of SCID mice (Figures 2E and S6). Thus, reprogrammed WS fibroblasts acquired infinite proliferative potential, and the ESC-like characteristics of the resulting iPSCs were maintained for more than 2 years.

Suppression of senescence-associated gene expression in WS iPSCs after long-term culture

Global gene expression analysis using DNA chips showed pronounced similarities among pluripotent stem cells including WS iPSCs. However, marked differences between WS iPSC and WS fibroblasts were observed (Figure S7). Heat map analysis also showed a high analogy of global gene expression profiles in these

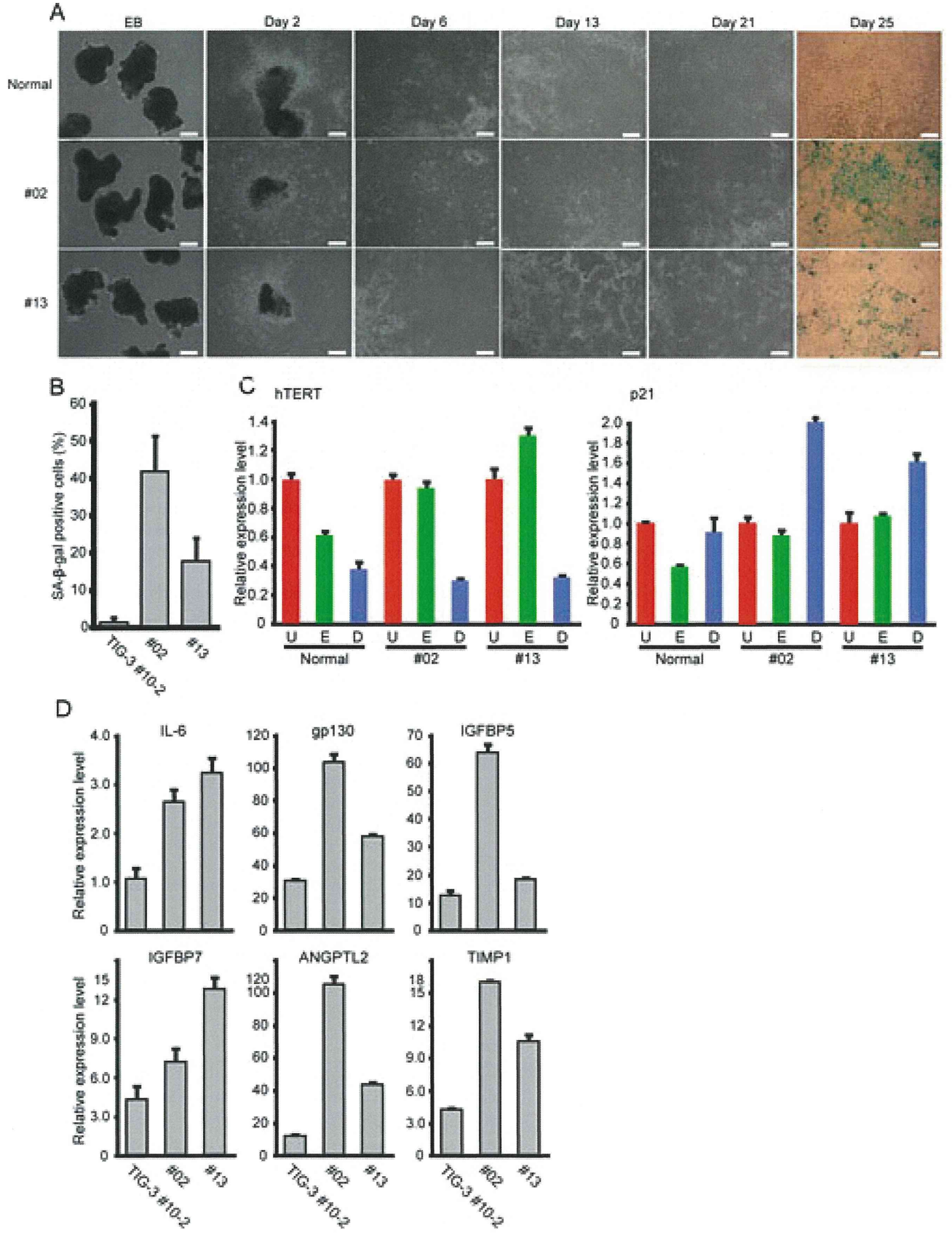

Figure 5. Recapitulation of Premature Senescence Phenotypes in Differentiated Cells from WS iPSCs. (A) Differentiation of EBs from normal (TIG-3) and WS (WSCU01 #02 and #13) iPSCs. Differentiated cells from WS iPSCs showed premature senescence. SA-β-gal staining was performed on day 25 of differentiation. Bars = 100 μm. (B) Percentage of senescent cells after 25 days of differentiation. SA-β-gal-positive cells were

counted in three randomly selected fields with 40× magnification. Values represent means of the three fields ± SD. (C) Expression of hTERT and p21 mRNAs in undifferentiated iPSCs ("U," red columns), EBs after 12 days of formation ("E," green columns), and differentiated cells after 25 days of differentiation ("D," blue columns). Values represent means of three technical replicates ± SD. (D) Expression of SASP genes in differentiated cells from normal (TIG-3) and WS (WSCU01 #02 and #13) iPSCs after 25 days of differentiation. Graphs shows fold changes relative to undifferentiated iPSCs. Values represent means of three technical replicates ± SD.
doi:10.1371/journal.pone.0112900.g005

pluripotent stem cell lines, but distinctly different profiles from those of WS fibroblasts (Figures S8A). Recent studies of aging have identified senescence-induced inflammatory and secretory factors that are collectively referred to as the senescence-associated secretory phenotype (SASP) and are the hallmarks of aging. It is widely accepted that age-associated inflammatory responses contribute to human aging mechanisms [26]. Accordingly, we observed downregulation of SASP secretory factors, including inflammatory cytokines, growth factors and MMPs, in both normal and WS iPSCs compared with WS fibroblasts (Figures S8B). Subsequently, we performed real-time qRT-PCR analysis using PDL-matched normal and patient fibroblasts, and their iPSC derivatives which were maintained in long-term culture. Although relative expression levels of the senescence-associated cyclin-dependent kinase inhibitor (CDKI) genes *p21Waf1/Cip1* and *p16INK4a* in normal fibroblasts correlated with the donor age, the expression levels of these genes were higher in WS fibroblasts than in normal fibroblasts, indicating that replicative senescence was prematurely induced in WS cells (Figure 3A). However, expression levels of these genes were significantly reduced in all iPSC clones from normal and WS cells (Figure 3A), suggesting that these gene loci are reprogrammed to the same degree in normal and WS iPSCs. Thus, we examined the expression of the typical SASP genes *IL-6* and *gp130* [27] and found higher expression levels in WS fibroblasts than in normal fibroblasts (Figure 3B). Moreover, expression levels of these genes drastically decreased in both normal and WS iPSCs compared with parental fibroblasts. Similarly, expression levels of the SASP genes *IGFBP5*, *IGFBP7*, *ANGPTL2*, and *TIMP1* ([28–31] were significantly decreased in both normal and WS iPSCs compared with parental fibroblasts (Figures 3B).

Reprogramming of the SASP gene loci is mediated by factors other than activated telomerase

WS fibroblasts were previously shown to bypass premature senescence following introduction of the telomerase gene *hTERT* [32], Similarly, the present WS cells bypassed premature replicative senescence, and hTERT allowed cell division for over 150 PDL in A0031 cells, and 40 PDL in WSCU01 cells compared with parental cells that became senescent at less than 30 PDL (Figures S9A and S9B). TRF length analysis showed that hTERT-expressing WS cells acquired longer telomeres during passages than parental cells (Figures S9C). To examine whether the expression of hTERT was sufficient to suppress the upregulation of aging-associated genes in WS cells, we compared expression levels of CDKI and SASP genes between WS fibroblasts and their hTERT-expressing derivatives. Whereas a decline in p21waf1/cip1 and p16INK4a mRNA expression was observed in hTERT-expressing cells (Figure 4A), IL-6 and gp130 expression was not suppressed following the introduction of hTERT, suggesting that reprogramming of the SASP gene loci is mediated by factors other than activated telomerase (Figure 4B). The present data show complete suppression of premature senescence phenotypes in WS cells using transcription factor-induced reprogramming and suggest that persistence of the undifferentiated state and pluripotency are crucial for reversing the aging process.

Recapitulation of premature senescence phenotypes in differentiated cells from WS iPSCs

To establish cell lineages that prematurely senesced, EBs consisting of equal numbers of iPSCs maintained in long-term culture were differentiated in serum-containing medium. Differentiated cells from WS iPSC-derived EBs were outgrown less rapidly than those from normal iPSC-derived EBs (Figure 5A, Day 2). These cells exhibited flat and enlarged morphology (Figure 5A, Day 6, 13, and 21) and became positive for SA-β-gal staining (Figure 5A, Day 25, and Figure 5B). Whereas expression levels of hTERT were downregulated equally in differentiated cells from normal and WS iPSCs, p21 mRNA was more highly induced in differentiated cells from WS iPSCs than those from normal iPSCs (Figure 5C). Expression levels of the SASP genes were also significantly increased in differentiated cells from WS iPSCs

Table 1. Results of chromosome analysis of WS iPSC clones and their parenral cells.

Cell lines	Numbers of cells analyzed by G-banding	Numbers of cells analyzed by M-FISH	Karyotypes
A0031	20 (13/7)	ND	46,XY,del(8)(q22q24)/46,XY,t(1;14)(p34.1;q13),t(4;7)(p15.2;q22),del(8)(q22q24)
iPS#23	20	10	46,XY,t(1;14)(p34.1;q13),t(4;7)(p15.2;q22),del(8)(q22q24),der(21)t(17;21)(?;q22.3)
iPS#34	20	10	46,XY,t(1;14)(p34.1;q13),t(4;7)(p15.2;q22),del(8)(q22q24)
iPS#64	20	10	46,XY,t(1;14)(p34.1;q13),t(4;7)(p15.2;q22),del(8)(q22q24),der(19)t(2;19)(?;p13.3)
WSCU01	20	ND	46,XY,normal
iPS#02	20	10	47,XY,+del(20)(p?)
iPS#13	20	10	46,XY,normal
iPS#14	20	10	46,XY,normal

Abbreviations: t, translocation; del, deletion; der, derivative chromosome; p, short arm; q, long arm.
doi:10.1371/journal.pone.0112900.t001

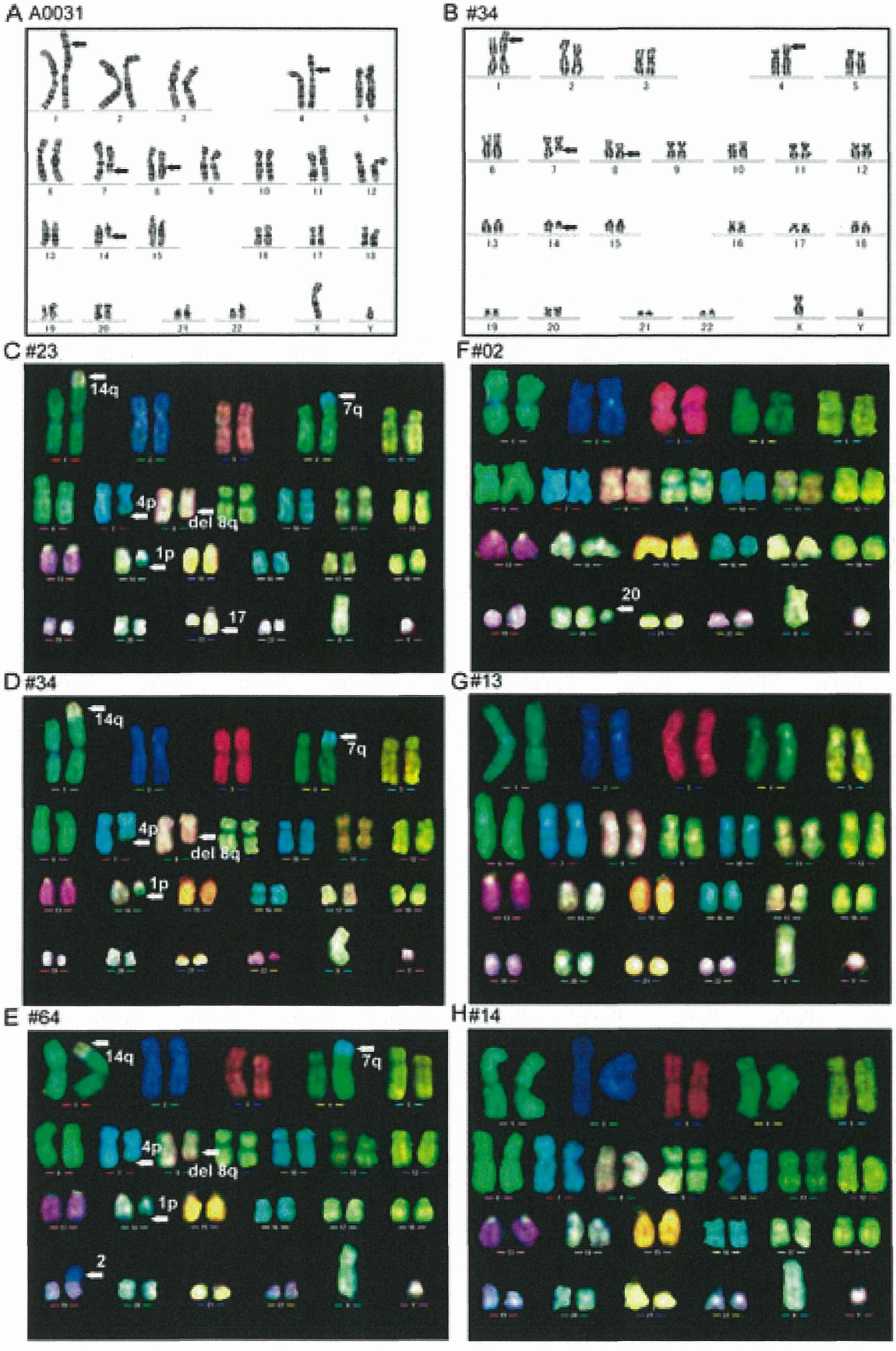
A A0031
B #34
C #23
14q
7q
4p
del 8q
1p
17
F #02
20
D #34
14q
7q
4p
del 8q
1p
G #13
E #64
14q
7q
4p
del 8q
1p
2
H #14

Figure 6. Karyotype Analysis of WS iPSCs. Chromosomal profiles of G-band analysis. (A) Parental A0031 fibroblast and (B) A0031-derived iPSC clone #34. Arrows indicate translocation breakpoints. Chromosomal profiles of M-FISH analysis. A0031-derived iPSC clones (C) #23, (D) #34, and (E) #64 and WSCU01-derived iPSC clones (F) #02, (G) #13, and (H) #14. Arrows indicate translocation breakpoints or an extra chromosome.
doi:10.1371/journal.pone.0112900.g006

compared with those from normal iPSCs (Figure 5D). These results demonstrated recapitulation of premature senescence phenotypes with downregulation of hTERT in differentiated cells from WS iPSCs.

Karyotype analysis of WS iPSCs

WS is characterized by genomic instability, and gene translocation events have been observed during culture of patient-derived cells [33]. Because reprogramming of somatic cells and subsequent maintenance of iPSCs involves extensive cell division, WS iPSCs may acquire additional chromosomal abnormalities. Thus, we compared chromosomal profiles of long-term cultured WS iPSC clones with those of parental WS fibroblasts by karyotype analysis. The subsequent G-banding stain and multicolor fluorescence *in situ* hybridization (M-FISH) analysis are summarized in Table 1.

Chromosomal profiles of parental A0031 WS fibroblasts showed mosaicism with the following abnormal karyotypes: 46, XY with a deletion in 8q and 46, XY with a deletion in 8q along with reciprocal translocations between 1p and 14q, and 4p and 7q (Figure 6A). These karyotypes support previous observations of chromosomal instability in WS cells [33]. Whereas, 1 of the derived iPSC clones (#34) had the same chromosomal profile as its parent cells (Figures 6B and 6D), the other 2 A0031-derived iPSC clones (#23 and #64) had the translocations 21q and 19p, respectively, in addition to those of the parental karyotype (Table 1, Figures 6C and 6E). Moreover, whereas parental WSCU01 fibroblasts and 2 of their derived iPSC clones (#13 and #14) had normal karyotypes (Table 1, Figures 6G and 6H), the remaining iPSC clone #02 carried the abnormal karyotype 47 (XY with an additional aberrant chromosome derived from chromosome 20; Table 1, Figure 6F).

The observation that 3 of 6 WS iPSC clones had the same karyotypes as their parental cells after approximately 100 passages suggests that karyotypes of WS cells are stabilized following reprogramming.

Discussion

In this study, we demonstrated that WS fibroblasts could be reprogrammed into iPSCs using Yamanaka factors, and the resulting iPSCs showed unlimited proliferative capacity that was sufficient for self-renewal over a period of 2 years. WS iPSCs also exhibited undifferentiated states and differentiation potential after long-term culture. Subsequently, we showed that WS iPSCs maintain immortality and ESC-like characteristics that indicate corrected telomere dysfunction following reprogramming of WS cells. Although WRN was not essential for generation of iPSCs, WRN helicase may protect genome integrity by mechanism other than the maintenance of telomere in iPSCs.

TRF length analysis indicated that WS iPSC lines maintained telomere with size variation in each clone. It is known that human iPSCs derived from normal somatic cells showed varied telomere length, and variation of telomere length among human iPSC clones is thought to partly depend on acquired telomerase activity associated with their reprogrammed states [34,35]. Therefore, variation of telomere length observed among WS iPSC clones would be due to clonal variation in telomerase activity rather than telomere dysfunction associated with *WRN* deficiency.

Normal human iPSCs are known to acquire genomic instability with a high incidence of additions, deletions and translocations [36,37]. In contrast, chromosomal aberrations are frequently caused by telomere dysfunctions in WS fibroblasts following the induction of cell cycle progression [11]. Nonetheless, the present data show unexpected maintenance of chromosomal profiles in WS iPSC clones during long-term culture for more than 100 passages although half of these clones acquired additional chromosomal abnormalities. Previously, the introduction of hTERT reduced the chromosomal aberrations in cells from WS patients [11]. In agreement, the present data indicate endogenous hTERT expression in WS iPSCs, but not in parental fibroblasts, suggesting that reprogramming suppresses chromosomal instability in WS cells by reactivating telomerase.

Previous studies show that WS fibroblasts express inflammatory cytokines [38] and WS is associated with inflammatory conditions such as atherosclerosis, diabetes and osteoporosis [39–43]. The present data indicate that both CDKI and SASP genes are prematurely induced in WS fibroblasts compared with PDL-matched normal fibroblasts. However, expression levels of these genes were completely suppressed in WS iPSCs to the same degree observed in normal iPSCs. In contrast, hTERT did not suppress SASP genes in WS fibroblasts, as shown by previous study [44], although a decline in p21waf1/cip1 and p16INK4a mRNAs was observed. Taken together, these observations suggest that pluripotency-associated transcription factor-induced reprogramming reverses the aging process in both normal and WS cells. Furthermore, differentiated cells from EBs of long-term cultured WS iPSCs showed premature senescence phenotypes, thus demonstrating that WS iPSCs stably maintained their potential to recapitulate premature senescence phenotypes during differentiation over the long term. In addition, embryoid body-mediated iPSC differentiation recapitulated premature senescence phenotypes in WS iPSCs, suggesting that it would provide a simple and rapid way to identify cell lineages affected in WS.

In the present study, we demonstrated the potential of WS iPSCs to proliferate infinitely and differentiate into various cell types, which could be used to provide patient cells in large quantities over the long term. Because WS-specific iPSCs may be differentiated into multiple cell types, their experimental use may resolve the major pathogenic processes of WS for which cell types available from patients are usually limited to lymphocytes and/or fibroblasts. The present technologies may also be used to develop cell transplantation therapies for WS patients using gene-corrected patient cells. The present observations indicate that WS iPSCs may be a powerful tool for understanding normal aging and the pathogenesis of WS.

Supporting Information

Figure S1 Generation of WS iPSCs. (A) Generation of iPSCs. Normal (TIG-3) and Werner syndrome (A0031 and WSCU01) fibroblasts are shown in the left panels, and emergence of morphologically distinct ESC-like colonies from parental cells is shown in the right panels. (B) Alkaline phosphatase activity of ESC-like colonies derived from TIG-3 and A0031 fibroblasts. (C) Colony morphologies of WSCU01-derived WS iPSC clones in early and late passages. Bars = 100 μm.
(EPS)

Figure S2 Evidences that WS iPSCs were derived from patients. (A) Western blot analysis of WRN helicase protein in WS iPSCs. (B) Direct sequencing analysis identified compound heterozygous mut.4/mut.6 mutations in WS iPSCs. Mut.4 is a C to G substitution at the splice-donor site bordered by exon 26, as shown by an arrow in the illustration of the double-strand base sequence. Obtained pherograms show antisense peak shapes. A peak corresponding to mut.4 in normal TIG-3 fibroblast shows a single "C," whereas the WS iPSC clone #34 from A0031 fibroblasts gave double peaks showing "G" in addition to "C." Mut.6 is a T to C substitution in exon 9. A peak corresponding to mut.6 in normal cells showed a single "C," whereas WS iPSC gave double peaks showing "T" in addition to "C." C, blue; G, black; T, red; A, green. (C) STR analysis of A0031-derived iPSC clone #34, showing that iPSC clone #34 was derived from the parental A0031 fibroblasts.
(EPS)

Figure S3 Expression of pluripotency genes in WSCU01-derived WS iPSC clones in early and late passages.
(EPS)

Figure S4 Expression of hESC markers in WS iPSCs in early and late passages. A0031-derived clones #34, and #64, and WSCU01-derived clones #02, #13, and #14 are shown. Bars = 100 μm.
(EPS)

Figure S5 Immunocytochemistry for differentiation of embryoid bodies into 3 germ layers for WS iPSCs in early and late passages. A0031-derived clones #34, and #64, and WSCU01-derived clones #02, #13, and #14 are shown. Bars = 100 μm.
(EPS)

Figure S6 Hematoxylin and eosin histology of teratomas derived from iPSCs. Hematoxylin and eosin histology of teratomas derived from iPSCs. The normal TIG-3 fibroblast-derived clone #10-2, A0031-derived clones #34, and #64, and the WSCU01-derived clone #02 are shown. Formation of all 3 germ layers is shown with melanin-producing cells and glial tissue (ectoderm), cartilage (mesoderm) and intestinal epithelia. Glands are lined by columnar epithelia and tracheal epithelium (endoderm).
(EPS)

Figure S7 Figure Scatter plots comparing gene expression profiles.
(EPS)

Figure S8 Analysis of senescence-associated gene expression in iPSCs. (A) Heat map analysis of WS iPSC #34 and parental WS A0031 fibroblasts, normal TIG-3 fibroblast-derived iPSCs, and hESC; 3277 probes with >5-fold differences in expression between A0031 fibroblast and WS iPSC were included in the heat map. (B) Heat map analysis of the gene profiles of secreted protein probes with >2-fold differences in expression between A0031 fibroblasts and the 3 pluripotent stem cell lines WS iPSC, TIG-3 iPSC, and hESC.
(EPS)

Figure S9 hTERT bypassed premature replicative senescence of WS fibroblasts. (A) Morphologies of growing normal TIG-3 fibroblasts, and A0031 and WSCU01 WS fibroblasts. WS fibroblasts showed premature senescence. SA-β-gal staining was performed for WSCU01 (lower). Bars = 100 μm. (B) Cumulative population doubling levels for hTERT-expressing WS cells. (C) TRF lengths of A0031 fibroblasts and their TERT-transduced derivatives.
(EPS)

Table S1
(EPS)

Table S2
(EPS)

Acknowledgments

We are grateful to Miho Kusuda-Furue (National Institute of Biomedical Innovation), Hidenori Akutsu (National Center for Child Health and Development) and Haruhiko Koseki (RCAI RIKEN) for their help, encouragement and suggestions. We also thank M. K. F and Bunsyo Shiotani for the critical review of draft manuscripts, and the Analysis Center of Life Science, Natural Science Center for Basic Research and Development of Hiroshima University for processing microarray data.

Author Contributions

Conceived and designed the experiments: AS. Performed the experiments: AS HK KZ YS YK MO MO HK TS KH HS YI KH YK. Analyzed the data: AS YK MO MO TS KH HS YI KH YK. Contributed reagents/materials/analysis tools: MG MT KY SY KF HT. Wrote the paper: AS MG. Final approval of the version to be published: AS HT.

References

1. Goto M, Miller RW, Ishikawa Y, Sugano H (1996) Excess of rare cancers in Werner syndrome (adult progeria). Cancer Epidemiol Biomarkers Prev 5: 239–246.
2. Goto M (2000) Werner's syndrome: from clinics to genetics. Clin Exp Rheumatol 18: 760–766.
3. Salk D, Au K, Hoehn H, Martin GM (1981) Effects of radical-scavenging enzymes and reduced oxygen exposure on growth and chromosome abnormalities of Werner syndrome cultured skin fibroblasts. Hum Genet 57: 269–275.
4. Yu CE, Oshima J, Fu YH, Wijsman EM, Hisama F, et al. (1996) Positional cloning of the Werner's syndrome gene. Science 272: 258–262.
5. Oshima J, Yu CE, Piussan C, Klein G, Jabkowski J, et al. (1996) Homozygous and compound heterozygous mutations at the Werner syndrome locus. Hum Mol Genet 5: 1909–1913.
6. Goto M, Imamura O, Kuromitsu J, Matsumoto T, Yamabe Y, et al. (1997) Analysis of helicase gene mutations in Japanese Werner's syndrome patients. Hum Genet 99: 191–193.
7. Matsumoto T, Imamura O, Yamabe Y, Kuromitsu J, Tokutake Y, et al. (1997) Mutation and haplotype analyses of the Werner's syndrome gene based on its genomic structure: genetic epidemiology in the Japanese population. Hum Genet 100: 123–130.
8. Shimamoto A, Sugimoto M, Furuichi Y (2004) Molecular biology of Werner syndrome. Int J Clin Oncol 9: 288–298.
9. Rossi ML, Ghosh AK, Bohr VA (2010) Roles of Werner syndrome protein in protection of genome integrity. DNA Repair (Amst) 9: 331–344.
10. Crabbe L, Verdun RE, Haggblom CI, Karlseder J (2004) Defective telomere lagging strand synthesis in cells lacking WRN helicase activity. Science 306: 1951–1953.
11. Crabbe L, Jauch A, Naeger CM, Holtgreve-Grez H, Karlseder J (2007) Telomere dysfunction as a cause of genomic instability in Werner syndrome. Proc Natl Acad Sci U S A 104: 2205–2210.
12. Takahashi K, Yamanaka S (2006) Induction of pluripotent stem cells from mouse embryonic and adult fibroblast cultures by defined factors. Cell 126: 663–676.
13. Takahashi K, Tanabe K, Ohnuki M, Narita M, Ichisaka T, et al. (2007) Induction of pluripotent stem cells from adult human fibroblasts by defined factors. Cell 131: 861–872.
14. Yu J, Vodyanik MA, Smuga-Otto K, Antosiewicz-Bourget J, Frane JL, et al. (2007) Induced pluripotent stem cell lines derived from human somatic cells. Science 318: 1917–1920.
15. Aoi T, Yae K, Nakagawa M, Ichisaka T, Okita K, et al. (2008) Generation of pluripotent stem cells from adult mouse liver and stomach cells. Science 321: 699–702.
16. Stadtfeld M, Hochedlinger K (2010) Induced pluripotency: history, mechanisms, and applications. Genes Dev 24: 2239–2263.

17. Okita K, Yamanaka S (2011) Induced pluripotent stem cells: opportunities and challenges. Philos Trans R Soc Lond B Biol Sci 366: 2198–2207.
18. Stadtfeld M, Maherali N, Breault DT, Hochedlinger K (2008) Defining molecular cornerstones during fibroblast to iPS cell reprogramming in mouse. Cell Stem Cell 2: 230–240.
19. Cheung HH, Liu X, Canterel-Thouennon L, Li L, Edmonson C, et al. (2014) Telomerase protects werner syndrome lineage-specific stem cells from premature aging. Stem Cell Reports 2: 534–546.
20. Batista LF, Pech MF, Zhong FL, Nguyen HN, Xie KT, et al. (2011) Telomere shortening and loss of self-renewal in dyskeratosis congenita induced pluripotent stem cells. Nature 474: 399–402.
21. Goto M, Ishikawa Y, Sugimoto M, Furuichi Y (2013) Werner syndrome: A changing pattern of clinical manifestations in Japan (1917~2008). Biosci Trends 7: 13–22.
22. Morita S, Kojima T, Kitamura T (2000) Plat-E: an efficient and stable system for transient packaging of retroviruses. Gene Ther 7: 1063–1066.
23. Amps K, Andrews PW, Anyfantis G, Armstrong L, Avery S, et al. (2011) Screening ethnically diverse human embryonic stem cells identifies a chromosome 20 minimal amplicon conferring growth advantage. Nat Biotechnol 29: 1132–1144.
24. Ohtaki K, Sposto R, Kodama Y, Nakano M, Awa AA (1994) Aneuploidy in somatic cells of in utero exposed A-bomb survivors in Hiroshima. Mutat Res 316: 49–58.
25. Debacq-Chainiaux F, Erusalimsky JD, Campisi J, Toussaint O (2009) Protocols to detect senescence-associated beta-galactosidase (SA-betagal) activity, a biomarker of senescent cells in culture and in vivo. Nat Protoc 4: 1798–1806.
26. Goto M (2008) Inflammaging (inflammation + aging): A driving force for human aging based on an evolutionarily antagonistic pleiotropy theory? Biosci Trends 2: 218–230.
27. Salama R, Sadaie M, Hoare M, Narita M (2014) Cellular senescence and its effector programs. Genes Dev 28: 99-114.
28. Kojima H, Kunimoto H, Inoue T, Nakajima K (2012) The STAT3-IGFBP5 axis is critical for IL-6/gp130-induced premature senescence in human fibroblasts. Cell Cycle 11:
29. Wajapeyee N, Serra RW, Zhu X, Mahalingam M, Green MR (2008) Oncogenic BRAF induces senescence and apoptosis through pathways mediated by the secreted protein IGFBP7. Cell 132: 363–374.
30. Tabata M, Kadomatsu T, Fukuhara S, Miyata K, Ito Y, et al. (2009) Angiopoietin-like protein 2 promotes chronic adipose tissue inflammation and obesity-related systemic insulin resistance. Cell Metab 10: 178–188.
31. Gilbert LA, Hemann MT (2010) DNA damage-mediated induction of a chemoresistant niche. Cell 143: 355–366.
32. Wyllie FS, Jones CJ, Skinner JW, Haughton MF, Wallis C, et al. (2000) Telomerase prevents the accelerated cell ageing of Werner syndrome fibroblasts. Nat Genet 24: 16–17.
33. Salk D, Au K, Hoehn H, Stenchever MR, Martin GM (1981) Evidence of clonal attenuation, clonal succession, and clonal expansion in mass cultures of aging Werner's syndrome skin fibroblasts. Cytogenet Cell Genet 30: 108–117.
34. Mathew R, Jia W, Sharma A, Zhao Y, Clarke LE, et al. (2010) Robust activation of the human but not mouse telomerase gene during the induction of pluripotency. FASEB J 24: 2702–2715.
35. Vaziri H, Chapman K, Guigova A, Teichroeb J, Lacher M, et al. (2010) Spontaneous reversal of the developmental aging of normal human cells following transcriptional reprogramming. Regen Med 5: 345–363.
36. Taapken SM, Nisler BS, Newton MA, Sampsell-Barron TL, Leonhard KA, et al. (2011) Karotypic abnormalities in human induced pluripotent stem cells and embryonic stem cells. Nat Biotechnol 29: 313–314.
37. Martins-Taylor K, Nisler BS, Taapken SM, Compton T, Crandall L, et al. (2011) Recurrent copy number variations in human induced pluripotent stem cells. Nat Biotechnol 29: 488–491.
38. Kumar S, Vinci JM, Millis AJ, Baglioni C (1993) Expression of interleukin-1 alpha and beta in early passage fibroblasts from aging individuals. Exp Gerontol 28: 505–513.
39. Murano S, Nakazawa A, Saito I, Masuda M, Morisaki N, et al. (1997) Increased blood plasminogen activator inhibitor-1 and intercellular adhesion molecule-1 as possible risk factors of atherosclerosis in Werner syndrome. Gerontology 43 Suppl 1: 43–52.
40. Yokote K, Hara K, Mori S, Kadowaki T, Saito Y, et al. (2004) Dysadipocytokinemia in werner syndrome and its recovery by treatment with pioglitazone. Diabetes Care 27: 2562–2563.
41. Rubin CD, Zerwekh JE, Reed-Gitomer BY, Pak CY (1992) Characterization of osteoporosis in a patient with Werner's syndrome. J Am Geriatr Soc 40: 1161–1163.
42. Davis T, Kipling D (2006) Werner Syndrome as an example of inflamm-aging: possible therapeutic opportunities for a progeroid syndrome? Rejuvenation Res 9: 402–407.
43. Goto M, Sugimoto K, Hayashi S, Ogino T, Sugimoto M, et al. (2012) Aging-associated inflammation in healthy Japanese individuals and patients with Werner syndrome. Exp Gerontol 47: 936–939.
44. Choi D, Whittier PS, Oshima J, Funk WD (2001) Telomerase expression prevents replicative senescence but does not fully reset mRNA expression patterns in Werner syndrome cell strains. FASEB J 15: 1014–1020.

OPEN ACCESS Freely available online

PLOS | ONE

Generation of Human Induced Pluripotent Stem (iPS) Cells in Serum- and Feeder-Free Defined Culture and TGF-β1 Regulation of Pluripotency

Sachiko Yamasaki[1], Yuki Taguchi[1], Akira Shimamoto[2], Hanae Mukasa[1], Hidetoshi Tahara[2], Tetsuji Okamoto[1]*

1 Department of Molecular Oral Medicine and Maxillofacial Surgery, Applied Life Sciences, Graduate Institute of Biomedical & Health Sciences, Hiroshima University, Japan, **2** Department of Cellular and Molecular Biology, Basic Life Sciences, Graduate Institute of Biomedical & Health Sciences, Hiroshima University, Japan

Abstract

Human Embryonic Stem cells (hESCs) and human induced Pluripotent Stem cells (hiPSCs) are commonly maintained on inactivated mouse embryonic fibroblast as feeder cells in medium supplemented with FBS or proprietary replacements. Use of culture medium containing undefined or unknown components has limited the development of applications for pluripotent cells because of the relative lack of knowledge regarding cell responses to differentiating growth factors. In addition, there is no consensus as to the optimal formulation, or the nature of the cytokine requirements of the cells to promote their self-renewal and inhibit their differentiation. In this study, we successfully generated hiPSCs from human dental pulp cells (DPCs) using Yamanaka's factors (*Oct3/4, Sox2, Klf4*, and *c-Myc*) with retroviral vectors in serum- and feeder-free defined culture conditions. These hiPSCs retained the property of self-renewal as evaluated by the expression of self-renewal marker genes and proteins, morphology, cell growth rates, and pluripotency evaluated by differentiation into derivatives of all three primary germ layers *in vitro* and *in vivo*. In this study, we found that TGF-β1 increased the expression levels of pluripotency markers in a dose-dependent manner. However, increasing doses of TGF-β1 suppressed the growth rate of hiPSCs cultured under the defined conditions. Furthermore, over short time periods the hiPSCs cultured in hESF9 or hESF9T exhibited similar morphology, but hiPSCs maintained in hESF9 could not survive beyond 30 passages. This result clearly confirmed that hiPSCs cultured in hESF9 medium absolutely required TGF-β1 to maintain pluripotency. This simple serum-free adherent monoculture system will allow us to elucidate the cell responses to growth factors under defined conditions and can eliminate the risk might be brought by undefined pathogens.

Citation: Yamasaki S, Taguchi Y, Shimamoto A, Mukasa H, Tahara H, et al. (2014) Generation of Human Induced Pluripotent Stem (iPS) Cells in Serum- and Feeder-Free Defined Culture and TGF-β1 Regulation of Pluripotency. PLoS ONE 9(1): e87151. doi:10.1371/journal.pone.0087151

Editor: Zhongjun Zhou, The University of Hong Kong, Hong Kong

Received August 30, 2013; **Accepted** December 19, 2013; **Published** January 29, 2014

Funding: This work was supported in part by research grants (no. 22659369 and 24890139) from the Japanese Ministry of Education, Culture, Sports, Science and Technology to TO and SY. The funders had no role in study design, data collection and analysis, decision to publish, or preparation of the manuscript.

Competing Interests: The authors have declared that no competing interests exist.

* E-mail: tetsuok@hiroshima-u.ac.jp

Introduction

Human somatic cells can be reprogrammed into induced pluripotent stem cells (iPSCs) by introduction of transcription factors such as *Oct3/4*, *Sox2*, *Klf4* and *c-Myc* [1]. Embryonic stem cells (ESCs) and human iPSCs (hiPSCs) can proliferate without limit and yet maintain the potential to generate derivatives of all three germ layers. These properties make them useful for understanding the basic biology of the human body, for drug discovery and testing, and for transplantation therapies. However, the original protocol for the derivation of hiPSCs required feeder cells and mouse embryonic fibroblasts (MEF) to provide a microenvironment for the reprogramming and the maintenance of hiPSCs [1,2]. Although it is known that MEFs produce a number of secreted protein factors, they are traditionally used for ES cell culture. The inclusion of uncharacterized animal protein supplements makes culture conditions more complex with increased variability in nutrients and factors that contribute to cell growth and the maintenance of pluripotency. Furthermore there is unavoidable variability in using live cells as feeders, which may affect reprogramming steps. For these reasons defined culture conditions without feeder cells are desirable. Although several defined culture conditions without feeder cells for hiPSCs have been reported, manipulation of undifferentiated hESCs and hiPSCs still remains problematic. For example, as we show below, hiPSCs cultured in serum-free and feeder-free conditions in the absence of exogenous TGF-β1 lose pluripotency with passaging over time.

Previously, feeder-free methods using FGF-2 and activin A for iPS cell derivation from adult fibroblasts using hESF9 medium [3] (Table S1) or using chemically defined conditions for hiPS cell derivation and culture [4] have been reported. In the present study, we adapted a method that has been established for hES cell culture, which uses FGF-2 and heparin with a defined medium formulation [5]. We have validated the same formula in the reprogramming of fetal lung fibroblasts (TIG-3) and adult dental pulp cells (DPCs) to iPSCs without feeder cells. At first, we examined whether hESF9 medium and each of three ECM (type I collagen, gelatin, fibronectin) -coated surfaces could be used for iPS cell derivation. Although each ECM could generate hiPSCs,

type I collagen and gelatin could not maintain the pluripotency of hiPSCs. Secondly, we performed retrovirus production using PLAT-A cells in serum-free conditions and analyzed transduction efficiency. From these results, we performed hiPS cell generation from patient-derived DPCs using hESF9 medium with fibronectin in completely serum-free culture conditions. The medium is capable of maintaining reprogrammed cells that expressed ES cell factors and retained the potential to differentiate into all three embryonic germ layers.

TGF-βs and their family members have been implicated in the development and maintenance of various organs in which stem cells play important roles. In hESCs, the predominant signaling pathways involved in pluripotency and self-renewal are TGF-β, which signals through Smad2, 3, 4, and FGFR, which activates the MAPK and Akt pathways. Signaling through these pathways results in the expression and activation of three key transcription factors: Oct3/4, Sox2, and Nanog. These transcription factors activate gene expression of ESC-specific genes, regulate their own expression and also serve as hESCs markers. To improve the stability of hiPSC pluripotency, we investigated the effect of TGF-β1. The addition of TGF-β1 to the defined serum-free medium for hiPSCs supported the robust proliferation and continued pluripotency of hiPSCs. Here we show that hESF9 medium in completely defined serum-free culture conditions supports the derivation and maintenance of pluripotent stem cells. This culture system will allow us to elucidate the cell responses to growth factors under defined conditions. These advantages will be beneficial for clarifying the molecular mechanisms of early development.

Materials and Methods

Ethics Statement

Written approval for human tissue collection and subsequent iPS cell generation and genome/gene analyses performed in this study was obtained from the Ethics Committee for Human Genome/Gene Analysis Research at Hiroshima University (approval number: hi-58), and written informed consent was obtained from each individual patient. All animal experiments in this study strictly followed a protocol approved by the Institutional Animal Care and Use Committee of Hiroshima University (approval number: A-11-140).

Cell culture of Dental pulp cell

Using a protocol approved by the Ethics Committee for Human Genome/Gene Analysis Research at Hiroshima University, we collected normal human third molars at Hiroshima University Hospital after having obtained informed consent for the usage of dental pulp cells (DPCs) to derive iPSCs. Primary human dental pulp cell cultures were established from dental pulp tissue discarded during surgery. The pulp tissue samples were minced into small clumps and then transferred into type I collagen (0.15 mg/ml) (Nitta gelatin, Osaka, Japan)- coated culture dishes in RD6F serum-free medium [11,12]. The cells were cultured at 37°C in a humid atmosphere of 5% CO_2. Fibroblastic cells that grew out from these colonies were digested in 0.05% trypsin-ethylenediaminetetraacetic acid (EDTA) in Ca^{2+} and Mg^{2+}-free phosphate-buffered saline (PBS), and the trypsin was inactivated with 0.1% soybean trypsin inhibitor (Sigma Aldrich, St. Louis, MO) in PBS. These cells were subcultured every 2-3 day.

Retrovirus production using PLAT-A packaging cell line

PLAT-A packaging cells [6] (Cell Bio Labs Inc., San Diego, CA) were seeded at 2×10^6 cells on collagen-coated flasks and cultured overnight in DMEM supplemented with 10% FBS. The next day, pMXs retroviral vectors (Add Gene, Cambridge, MA) containing the open reading frames of *Oct3/4*, *Sox2*, *Klf4*,*c-Myc* and *EGFP* were transfected into PLAT-A cells with Xtreme GENE HP Transfection Reagent (Roche Diagnostics, Cambridge, MA). After 48 hr the medium was completely changed to serum-free hESF9. Viral supernatants were collected 48 h to 72 h after transfection, filtered through a 0.45 μm pore size PVDF filter (Millex-HV, Millipore, Billerica, MA) and supplemented with 8 μg/ml Polybrene (Sigma). The DPCs were transduced with *Oct3/4*:*Sox2*:*Klf4*:*c-Myc* (1:1:1:1) mixture of viral supernatant. To determine the viral transduction efficiency of individual factors, *EGFP* transduced retrovirus supernatant was transduced to DPCs. Medium was changed every other day, and the cells cultured for 4 days. The cells were trypsinized and analyzed by flow cytometry (FACS Calibur™) (BD Biosciences, San Jose, CA).

The generation of hiPS cell using TIG-3 under feeder- and serum-free, defined culture conditions from the reprogramming step

To obtain iPSCs, TIG-3 (derived from fetal lung fibroblasts and purchased from the Health Science Research Resources Bank, Osaka, Japan) [7] cultured in DMEM supplemented with 10% FBS were transduced with the pMXs-based retroviral vectors encoding human *Oct3/4*, *Sox2*, *Klf4* and *c-Myc*, as described above. At the same time, TIG-3 were transduced the EGFP-expressing retroviral vector or the control vector with a constant amount of total DNA. After 4 days cells were photographed under a fluorescence microscope and analyzed by flow cytometry (FACS Calibur™). After 4 days cells transduced with the four factors were trypsinized and plated on 0.1% gelatin- (Millipore), or type I collagen- (0.3 mg/ml) (Nitta gelatin) or fibronectin- (2 μg/cm^2) (Sigma) coated dishes in hESF9 medium. For comparison, we used KSR-based medium and mitomycin C-treated MEF (Embryo Max® PMEF-H, Millipore) [8–10] as feeder cells (KSR-based conditions)[1,2]. After 20 days, we detected colonies that were subsequently passaged and maintained in hESF9 medium with individual ECMs. After 36 days of culture, ALP–positive colonies were counted.

Retrovirus Production using PLAT-A cell in serum-free conditions and transduction efficiency

Retroviral supernatants of pMXs-(empty) and pMXs-(EGFP) were produced in PLAT-A packaging cells in hESF9 medium or DMEM supplemented with 10% FBS. These collected virus supernatants were used for infection. After 3 days, infected TIG-3 cells were photographed under a fluorescence microscope and transduction efficiency analyzed by FACS Calibur™ of EGFP expression.

Generation of hiPS Cells from DPCs in completely defined culture conditions

DPCs were seeded at 3×10^5 cells per 60-mm dish in RD6F serum-free medium [11,12] and cultured overnight. The next day the cells were infected with viral supernatant for 24 h in hESF9 medium. Four days after transduction, these infected cells were harvested by trypsinization and seeded on fibronectin (2 μg/cm^2) (Sigma F-1141) -coated dishes at 1×10^5 cells per 100 mm dish in hESF9-medium. The medium was changed every other day. Approximately 20 days after infection, iPS colonies were picked based on human ES cell-like colony morphology. The picked colonies were subsequently expanded and maintained on fibronectin in hESF9T medium. Reprogramming efficiency was determined as the positive number of total ES-like ALP positive

colonies per total number of infected cells. Thirty-three days after transduction, we detected hiPSC-like colonies by ALP substrate staining. As a control, transduced DPCs were seeded on mitomycin-C-treated MEF feeder cells with KSR-based conditions [1,2].

Maintenance of human iPS cells in serum-free culture conditions

For subculturing colonies were mechanically detached from the culture dish and dissociated into small clamps by pipetting. The cell suspension was transferred on fibronectin-coated dishes in hESF9 medium or hESF9 with TGF-β1 (2 ng/ml) (R&D systems, Minneapolis, MN) (hESF9T). We defined this stage as passage 1. The medium was changed daily with hESF9T medium.

Cell growth analysis of human iPS cells generated and maintained in define culture conditions

Human iPSCs generated under hESF9 and cultured in hESF9T (DP-F-iPS-CL8 passage 38, DP-F-iPS-CL4 passage 38, DP-F-iPS-CL16 passage 33) were seeded in a 24-well plate coated with fibronectin and counted every 24 hr. Growth curves were calculated from each passage split ratio. The hiPSC colonies (DP-F-iPSCs) cultured for 1 month in feeder-free hESF9 or hESF9T were detached using a cell scraper and 0.001% trypsin-0.01% ethylenediaminetetraacetic acid (EDTA). The dissociated cells were then fixed, incubated with Alexa Fluor 647®-conjugated SSEA4 antibody or PerCP-Cy5.5-conjugated Oct3/4, and subjected to flow cytometry (FACS Aria™).

Alkaline phosphate (ALP) staining and Immunocytochemistry

Alkaline phosphatase staining was performed using a Fast Red substrate kit (Nichirei Biosciences Inc., Tokyo, Japan). To detect pluripotent stem cell marker antigens cells were fixed with PBS containing 4% paraformaldehyde for 10 min at room temperature. After washing with PBS, the cells were treated with PBS containing 5% normal goat serum (Nichirei) and 0.1% Triton X-100 for 45 min at room temperature. Fixed cells were stained with primary antibodies included SSEA-4 (1:100, Stemgent®, Cambridge, MA), TRA-1-60 (1/200, Stemgent®), TRA-1-81 (1/200, Stemgent®), Oct-3/4 (1/200 Millipore), Nanog (1/600, ReproCELL, Yokohama, Japan), Nestin (1/200, Millipore), βIII-tubulin (1/200, Millipore), α-smooth muscle actin (pre-diluted, DAKO Cytomation, Glostrup, Denmark) and α-fetoprotein (1/100, R&D Systems). These primary antibodies were visualized with Alexa Fluor® 488- conjugated goat anti-rabbit IgG, or Alexa Fluor® 594-conjugated goat anti-rabbit IgG, or Alexa Fluor® 488-conjugated goat anti-mouse IgG, or Alexa Fluor® 594-conjugated goat anti-mouse IgG (1/200, Invitrogen, Carlsbad, CA). Nucleuses were stained with DAPI. Fluorescence images were acquired using a Zeiss inverted LSM confocal microscope (Carl Zeiss, GmbH, Germany).

RNA isolation and reverse transcription gene expression

A detailed reverse transcription-polymerase chain reaction (RT-PCR) protocol was described previously [13]. Briefly, total RNA was extracted from iPSCs using the Illustra RNA spin Mini Isolation kit (GE Healthcare UK Ltd, Buckinghamshire, England), according to manufacturer's instructions. cDNA was synthesized from 1 μg of total RNA using High capacity RNA-to cDNA master mix (Applied Biosystems, Carlsbad, CA). RT-PCR was performed with AmpliTaq Gold DNA polymerase with Gene Amp (Applied Biosystems). The primers used in this study are described in Table S2. PCR products were size-fractionated using 1.5% agarose gel electrophoresis. DNA markers were used to confirm the size of the fragments.

Droplet digital PCR analysis

Droplet digital PCR (ddPCR) analysis was performed using QX100™ Droplet Digital™ PCR (Bio-RAD Laboratories, Hercules, CA). Total RNA was extracted from hiPSCs, and RT-PCR was performed. cDNA samples, primers and probes with the ddPCR master mix (Bio-Rad) were combined in water-oil emulsion droplets. These droplets were subjected to 40 PCR cycles. Positive and negative fluorescent droplets in each sample were detected with a QX100 Droplet reader (Bio-Rad). The relative mRNA expression in each sample was normalized to its GAPDH content. The mRNA levels in each cells were expressed relative to those in hESF9 medium (TGF-β1; 0 ng/ml), which was taken as 1. The results are presented as means±SD of three independent experiments.

Embryoid body formation

In vitro differentiation was induced by the formation of embryoid bodies as described previously [5]. Briefly, undifferentiated human DP-iPSCs were cultured in DMEM with 10% FBS for 4 days in low-attachment 96 well plates. After 4 days in suspension culture, floating embryoid bodies were re-seeded onto gelatin-coated dishes in the same culture medium for 10 days. The medium was changed every other day.

Teratoma formation assay and histological analysis

Human DP-iPSCs were suspended at 2×10^7 cells/ml in PBS and injected 50 ul of the cell suspension (1×10^6 cells) subcutaneously into dorsal flank of SCID (CB17/Icr-*Prkdc*^{scid}/CrlCrlj) mice. Ten weeks after the injection, tumors were surgically dissected from the mice. Teratomas were weighed, fixed in PBS containing 4% formaldehyde, and embedded in paraffin. Sections were stained with hematoxylin and eosin and Alcian Blue stain.

Short tandem repeat DNA analysis

Genomic DNA was used for PCR with Powerplex 16 system (Promega Corporation, Madison, WI) and analyzed by ABI PRISM 3100 Genetic analyzer and Gene Mapper v3.5 (Applied Biosystems).

RNA expression array analysis

A heat map generated from the RNA expression array data displayed the expression profile of the hESC-enriched genes and the differentiated cell-enriched genes. The genes shown in blue represented the down-regulation of gene expression, whereas the genes shown in red represented the up-regulation of gene expression. RNA expression array were performed using the Agilent Sure Print G3 Human GE 8x60K v2 Microarray, and data were analyzed using Genespring12.0 (Agilent Technologies, Santa Clara, CA).

Results

The generation of hiPS cells using TIG-3 under feeder- and serum-free, defined culture conditions from the reprogramming step

We examined whether hESF9 medium and each of three ECM (type I collagen, gelatin, fibronectin)-coated surfaces could be used for iPS cell derivation. We used Platinum-A retroviral packaging cell, amphotropic (PLAT-A) [6] carrying the *Oct3/4, Sox2, Klf4*